Rathi et al. *NPG Asia Materials* (2023) 15:70
https://doi.org/10.1038/s41427-023-00516-6

NPG Asia Materials

REVIEW ARTICLE Open Access

Hemozoin in malaria eradication—from material science, technology to field test

Ashutosh Rathi[1,2], Z. Chowdhry[1,2], Anand Patel[1,3], Siming Zuo[4], Thulya Chakkumpulakkal Puthan Veettil[5], John A. Adegoke[5], Hadi Heidari[4], Bayden R. Wood[5], Vidya Praveen Bhallamudi[1,2,3] and Weng Kung Peng[6]

Abstract

Malaria continues to be among the most lethal infectious diseases. Immediate barriers include the detection of low-parasitemia levels in asymptomatic individuals, which act as a reservoir for future infections, and the emergence of multidrug-resistant strains in malaria-endemic, under-resourced regions. The development of technologies for field-deployable devices for early detection and targeted drugs/vaccines is an ongoing challenge. In this respect, the identification of hemozoin during the Plasmodium growth cycle presents a unique opportunity as a biomarker for malaria infection. The last decade has witnessed the development of numerous opto-/magnetic- based ultrasensitive hemozoin sensing technologies with tremendous potential of rapid and accurate malaria diagnosis and drug testing. The unique information in hemozoin formation can also shed light on the development of targeted drugs. Here, we present a comprehensive perspective on state-of-the-art hemozoin-based methodologies for detecting and studying malaria. We discuss the challenges (and opportunities) to expedite the translation of the technology as a point-of-site tool to assist in the global eradication of malaria infection.

Introduction

Malaria is one of the most lethal and prevalent infectious diseases, which continues to cause the deaths of around half a million people each year.[1] To achieve the fast-approaching United Nations Sustainable Development Goal of global malaria elimination by 2030,[2] two processes i.e., accurate (specific and quantitative) diagnosis and appropriate (targeted drug) treatment, are crucial. Low-density malaria parasitemia in asymptomatic individuals at the early stage of infection goes undiagnosed or unnoticed, which serves as a reservoir for future infections and hinders the breaking of disease transmission. Nevertheless, the past two decades have witnessed unprecedented success in reducing the mortality rate. These efforts, however, were hampered by the growing parasites' resistance strains to common antimalarial drugs in endemic, under-resourced regions.[1,3] Additionally, the global spread of the COVID-19 pandemic in early 2020 jammed the healthcare system, putting a soft halt in the fight against malaria. In a likely reflection of this, devastating numbers of malaria deaths have been reported in 2020,[4] and the first malaria vaccine, despite its modest efficacy, was approved by the World Health Organization in 2021.[4,5] While malaria has always been prevalent in tropical and sub-tropical regions (e.g., sub-Saharan Africa), the increasing human mobility (e.g., travel and migration) poses a threat of malaria resurgence in traditionally non-endemic areas (e.g., United States and Europe).[6] Altogether, it is essential to take proactive measures to avoid being caught off-guard in any unforeseen upsurge of malaria, considering that the threat posed by COVID-19 still persists. This preparedness is especially

Correspondence: Ashutosh Rathi (rathi.medphy@gmail.com) or Hadi Heidari (hadi.heidari@glasgow.ac.uk) or Bayden R. Wood (wood@monash.edu) or Vidya Praveen Bhallamudi (praveen.bhallamudi@iitm.ac.in) or Weng Kung Peng (pengwengkung@sslab.org.cn)
[1]Quantum Center of Excellence for Diamond and Emergent Materials, Indian Institute of Technology Madras, Chennai 600036, India
[2]Department of Physics, Indian Institute of Technology Madras, Chennai 600036, India
Full list of author information is available at the end of the article
These authors contributed equally: Hadi Heidari, Bayden R. Wood, Vidya Praveen Bhallamudi, Weng Kung Peng

Table 1 SWOT analysis for different classes of malaria diagnosis.

	Microscopy	Molecular method	Serological based	Hemozoin sensing
Strength	Low-cost, field deployable, quantitative, species and stage identification	High sensitivity and specificity, high throughput, species identification	Low-cost, easy to operate, shorter diagnosis time, field deployable	high sensitivity, increased specificity, quick result, quantitative
Weakness	Limited sensitivity, labor intensive, Requires expertise, time-consuming	Highly time-consuming, bulky laboratory setting, expensive, labor-intensive	Limited sensitivity, less specificity, lack of heat stability, qualitative	Data governance and control, model maintenance
Opportunity	Skills of the microscopists in non-endemic settings, mobile application	Epidemiology studies	Non-*P. falciparum* species discrimination, multiplexing variants detection	Field deployable, lab on a chip, non-invasive, point-of-care diagnosis, species and stage identification
Threat	Low throughput	Over-reliance or phase-out?	HRPII deletion mutation (false negative), persistent antigen from past infections (false positive)	Expertise required?

crucial for remote, low-resource settings where malaria is already endemic.[7,8]

The ability of rapid and accurate diagnosis at the level to detect asymptomatic carriers, ideally <0.0001% parasitemia (≈5 parasites/μL of blood), will significantly impact disease transmission dynamics, and therefore, have a positive impact on the malaria elimination program.[9] The gold standard in malaria diagnosis, microscopic examination of Giemsa-stained infected red blood cells (i-RBCs) on a glass slide, remains unchanged for over a hundred years. Although the methodology is low-cost, quantitative, and parasite-specific, it is labor-intensive and time-consuming (around 1 h), and an average microscopist can only detect 0.001% parasitemia. Therefore, the search for detection methods at the sub-microscopic level with a speedy result remains a topic of high significance in malaria research.

Other clinically employed and emerging diagnostic technologies can be broadly categorized based on the target molecule, such as organic (e.g., protein and DNA/RNA) and inorganic (e.g., hemozoin). The methodologies adopted for the former are further classified into molecular-based techniques e.g., polymerase chain reaction (PCR), and serological-based techniques e.g., rapid diagnostic test (RDT).[10] PCR-based methods offer highly reliable and sensitive detection of < 0.0001% parasitemia, but are extremely slow to assess (at least in 2 h), costly, and require laboratory infrastructure, limiting their practicality for on-site application or limited medical-resources settings in under-developed or developing countries. Toward this end, low-cost and easy-to-use RDTs, based on lateral-flow immunoassay of parasite-specific antigens (e.g., HRPII and pLDH), offer moderately speedy malaria detection in less than 20 min, but the method lacks high accuracy (specificity) and does not even have the same level of sensitivity as light microscopy. Moreover, false positives due to the persistence of antigens for an extended period (after the infection has been cleared), false negatives, and no species identification (in the absence of HRPII), along with an inability for quantitative analysis, limit the performance and derived information from RDTs. Finally, RDTs generally require refrigeration, which is not suited for deployment in remote, under-resourced regions. Details and recent developments in these methodologies are discussed elsewhere.[10–13]

Individually, the current diagnostic tests (e.g., light microscopy, molecular approaches, serological tests, and RDTs) are not perfect for rapid (within a few minutes) and highly specific diagnoses at low (<0.0001%) parasitemia levels to detect asymptomatic carriers [see Table 1 and Fig. 1]. To this end, the scientific community in malaria research has paid great attention to interdisciplinary research on cutting-edge technologies focusing on inorganic malaria pigment, hemozoin,[14] which also provides a wide variety of information not available in traditional methods. Hemozoin, formed in an intra-erythrocyte cycle of the malaria parasite, is rich in magnetic and optical properties. Based on these characteristics, the identification of hemozoin presents a unique opportunity for malaria diagnosis and also provides the ability to analyze hemozoin formation, which may play a vital role in the testing and discovery of new targeted antimalarial drugs.

In the past decade, numerous hemozoin sensing technologies have been developed and refined for nearly ideal diagnostic characteristics, including ultra-sensitivity, high specificity, rapid result, and cost-effectiveness. Some of these technologies have already been tested in animal studies and in the field. Additionally, hemozoin-based

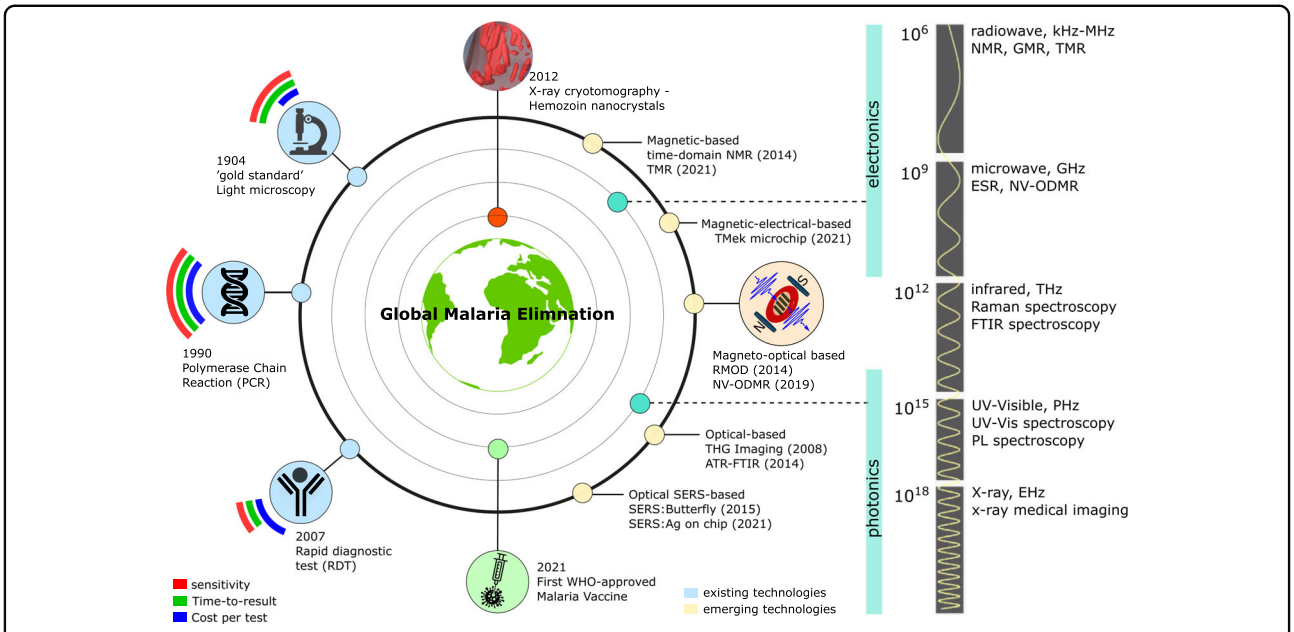

Fig. 1 Milestones for the development of technological innovations (i.e., photonic and electronic) toward global malaria elimination. A classification of methods for malaria diagnostics in the intra-erythrocyte cycle. The gold standard light microscopy has been used for more than a century in clinical settings, while molecular-based polymerase chain reaction (PCR) and serological-based rapid diagnostic test (RDT) techniques are more recent. These methods[10] are compared qualitatively for sensitivity (high, low), time-to-result (long, short), and cost per test (high, low). In the background of emerging spectroscopy-based technologies (photonics and electronics) under the action of electromagnetic radiation (nondestructive nature), more (clinical) information can be harvested. These techniques exploit the magnetic and optical properties of "inorganic" malaria pigment, hemozoin nanocrystals. Alongside the emergence of novel hemozoin sensing technologies aiming at on-site malaria diagnosis in asymptomatic individuals to faint transmission dynamics worldwide, the approval of the first of its kind, for any parasitic disease, malaria vaccine by the World Health Organization (WHO) in 2021, may play a significant role in reducing the severe malaria cases prevalent in <5-year-old children and pregnant women exposed to high transmission rates in WHO African Region. The X-ray cryotomography of hemozoin crystals was adapted with permission from ref. [46] Copyright: 2012, National Academy of Sciences.

sensing has been realized with microdevices, particularly lab-on-a-chip for point-of-care diagnostics, and can also offer noninvasive diagnostics, as reviewed elsewhere.[15–19] Furthermore, expert reviews on magnetophoretic[20] and optical methods[21–23] have been added to the literature at different times. Nonetheless, there remain plenty of fundamental questions to address (e.g., background signals from whole blood[24]), and further developments (e.g., machine learning) are still needed to facilitate easier decision-making for a more specific malaria diagnosis. At the bottom, the underlying mechanism for hemozoin formation is still not entirely clear, which is particularly important for the development of new targeted drugs.

We identified underlying questions and shed light on possible actions to develop an optimal malaria diagnostic tool and targeted antimalarial drugs, thereby advancing hemozoin-based technologies to a clinical platform. The article is structured to emphasize each aspect of hemozoin, ranging from its fundamental structure to its use in technology for global malaria elimination. Section "Biochemistry of malaria: hemozoin nanocrystals" covers the formation of hemozoin in the intra-erythrocyte cycle and recent progress in imaging the underlying mechanisms to assist in the development of new targeted drugs. Section "Magnetism of hemozoin: a double-edged sword" explores the magnetism of solitary hemozoin and its enigmatic nature (paramagnetic or superparamagnetic), as well as the resultant changes in magnetic characteristics from healthy to malaria-infected blood. In Section "Hemozoin sensing technologies", we introduce hemozoin sensing technologies, encompassing "Magnetic-based technology" and "Optical-based technology", and advanced methods based on the "Magneto-Optical based technology" optical detection of the magnetic fingerprints of hemozoin. We provide an up-to-date review of the various successes achieved using these different modalities. Section "Field evaluation" compares the performance of hemozoin detection technologies, specifically in field testing, with existing clinical methods serving as reference standards. In Section "Outlook", we present our perspective on challenges with hemozoin-based diagnostics and outline future directions to expedite the translation of these technologies into actual field implementation. Section "Concluding remarks" will offer concluding remarks on the current status of this research field.

Biochemistry of malaria: hemozoin nanocrystals

Malaria is a mosquito-borne disease caused by parasites of the genus Plasmodium,[25,26] which proliferate in an intra-erythrocytic (asexual) cycle from the ring stage to trophozoite and eventually to the replicating schizont stage (and so on) [see Fig. 2]. In an acidic lysosome-like organelle, known as the food or digestive vacuole (DV), the parasites cause proteolysis of erythrocytic hemoglobin (Hb)[27,28] as a principal nutrient source, releasing Fe^{2+}-centered heme,[29] which instantaneously oxidizes to by-product Fe^{3+}-containing (free) heme. To mitigate the high cytotoxicity of free heme, the parasites convert it into a physiologically insoluble product called hemozoin.[30] Thus, hemozoin formation is a vital process for the survival of Plasmodium parasites, and the underlying mechanism is crucial to understanding the modes of action of antimalarial drugs and searching for new possibilities.[31–33]

Hemozoin was long considered to be a linear coordination polymer[34,35] of (oxidized) heme molecules. However, the X-ray diffraction study[36] confirmed its crystalline nature with triclinic symmetry, resulting from cyclic dimerization of porphyrin rings via iron carboxylate links, followed by the intra-molecular hydrogen bonding to form a crystal [see Fig. 2]. The low crystal (triclinic) symmetry favors *unidirectional* growth [along (100) axis], giving rise to a high aspect ratio parallelogram or needle-like shape with a long-axis dimension in the sub-micrometer range. The crystal morphology changes moderately for different Plasmodium species and developmental stages.[37] However, the mechanisms governing hemozoin nucleation and growth remain enigmatic. Initially, the hemozoin crystal nucleation mechanism was suggested to be nonenzymatic and autocatalytic (physicochemical),[38,39] with crystal growth occurring over "preformed" β-hematin (consisting of one unit of hydrogen-bonded heme molecules). Soon, several in vitro studies highlighted the involvement of neutral lipids in hemozoin formation. These studies suggested hemozoin nucleation and growth within neutral lipid nanospheres in DV,[40] acylglycerol suspensions,[41] and acylglycerol lipid-solution interfaces.[42,43] Another study[44] hypothesized the existence of double-membrane hemoglobin transport vesicles (HTVs), consisting of the outer parasitophorous vacuole (PV) and the inner parasite plasma membrane (PPM). Hemoglobin digestion occurs inside the PPM, while heme biomineralization takes place on the surface. These HTVs eventually fuse with the DV.

Two pioneering reports by Kapishnikov et al.[45,46] clarified the nature of the growth medium. The first study using nanoprobe beam X-ray Fe-fluorescence and diffraction[45] revealed a clustering of hemozoin crystals with parallel alignment (of needle *c*-axes) such that (100) crystal faces were exposed to a curved surface. This suggests hemozoin nucleation via a common template and thus, excludes the process within lipid droplets. The companion study, employing high-contrast cryo soft X-ray tomography (cryo-XT) and electron microscopy,[46] addressed the questions related to the curved surface and HTVs hypothesis. The study confirmed the DV inner membrane as the common template for (100) oriented hemozoin nucleation. While the study also observed HTVs as uniform dark spheres, no hemozoin crystals were detected within the HTVs or along their pathway to the DV [see Fig. 2]. Additionally, the authors investigated the chemical environment of hemozoin crystallization and found it to occur in an aqueous milieu without any signature of lipid droplets enclosing the hemozoin crystals. This is further confirmed in their recent study with cryo-scanning transmission electron tomography in situ.[47]

Moreover, several parasite proteins, such as heme detoxification protein (HDP),[48] and its association with falcipain 2 (a major hemoglobinase) in a multiprotein complex in *Plasmodium falciparum*,[49] are shown to be extremely potent for hemoglobin degradation and hemozoin formation processes. Another important Plasmodium parasite-secreted protein is lipocalin-like PV5, which plays a crucial role in the development of asexual blood-stages in malaria.[50] A recent in vivo electron microscopy study[51] further demonstrated the significance of PV5 in the degree of heme biomineralization and, more importantly, in the regulation of hemozoin crystal unidirectionality. In *Plasmodium berghei* (in mice), PV5 transcriptional deregulation reduces hemozoin production, but this also causes an excessive elongation of hemozoin crystals. Conversely, its inactivation in *P. falciparum* results in the formation of hemozoin crystals with multidirectional branching. This study also supports the picture of hemozoin crystallization occurring within the aqueous milieu of the parasite's DV. Regardless of considerable changes in crystal morphology when PV5 is perturbed, electron diffraction experiments reveal an unaltered crystalline property, thus excluding a significant role of PV5 in hemozoin nucleation. Therefore, future studies are needed to understand hemozoin formation clearly to expedite the targeted drug development efforts.

Magnetism of hemozoin: a double-edged sword

Iron (Fe) is one of the few elements that possess ferromagnetic (FM) properties at room temperature. Given the rich elemental content of Fe in hemoglobin in RBCs, magnetic techniques have become an apparent choice for studying blood. In a seminal work in the 1930s on magnetism in blood, Pauling and Coryell[52,53] found Fe^{2+} (low-spin $S = 0$, diamagnetic) in oxyhemoglobin (oxy-Hb), Fe^{2+} (high-spin $S = 2$, paramagnetic) in deoxyhemoglobin (deoxy-Hb), whereas Fe^{3+} (high-spin $S = 5/2$, paramagnetic) in methemoglobin (met-Hb). In 1964, Weiss

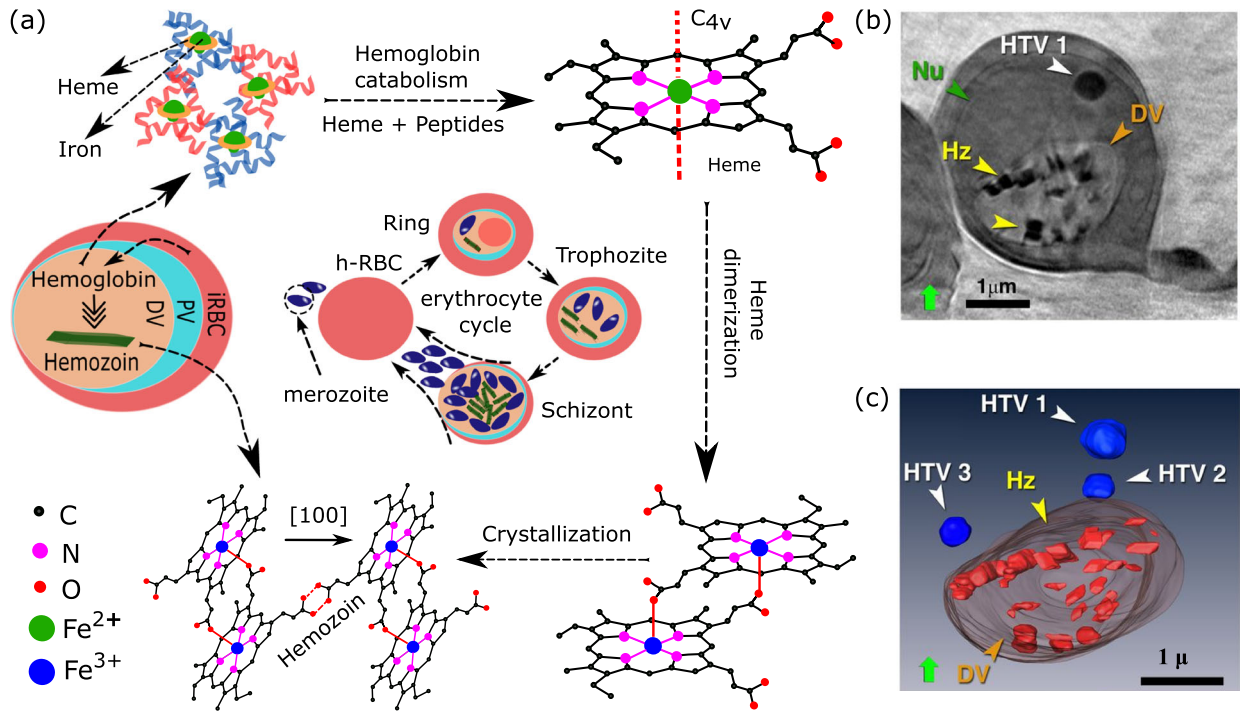

Fig. 2 Malaria pathogenesis, hemozoin biomineralization, and high-resolution microscopy. Malaria infection starts with the ingestion of Plasmodium parasite sporozoites [only *P. falciparum* (Pf), *P. vivax* (Pv), *P. malariae* (Pm), *P. ovale* (Po) and *P. knowlesi* (Pk) species are responsible for human malaria]. These sporozoites rapidly grow inside liver cells (hepatocytes) over a period of 6 days (for most virulent species, *P. falciparum*) or longer (clinically silent) before producing thousands of hepatic merozoites in the erythrocytes (disease-causing and sexual stage for malaria transmission to uninfected mosquitos). Hemozoin formation: (**a**) Upon invasion into healthy red blood cells (h-RBCs), merozoites (inside parasitophorous vacuole (PV)) digest hemoglobin in the digestive vacuole (DV) to facilitate the acquisition of peptides or amino acids for maturation, disentangling "porphyrin" cofactor Heme, chemically Fe^{2+}-protoporphyrin IX, from globin chains into infected red blood cells (i-RBCs). The porphyrins (with C_{4v} symmetry) in heme instantaneously undergo self-dimerization via Fe^{3+}-O (ironcarboxylate) bonds, resulting in its oxidized form, Fe^{3+}-protoporphyrin IX (hematin or free heme), a highly toxic product to the malaria parasites. In a detoxification process, the heme molecules are assembled via intra-molecular hydrogen bonds, forming an insoluble and bioinert inorganic crystal called hemozoin (chemically equivalent to *β*-hematin), which is a distinctive feature of i-RBCs and offers opportunities for malaria diagnostics and discovery of antimalarial drugs. All hydrogen atoms are omitted for clarity. Malaria cycle: In the erythrocytic stage, malaria parasites uni-nucleate and grow into a ring-like shape (within 6 h) and then transform into a trophozoite (within 24 h) and soon into a multi-nuclei schizont stage (within 36 hours). In the 48-h time period of the erythrocyte stage, the i-RBCs eventually rupture and release new merozoites, which further capture h-RBCs and the cycle repeats. *Cryogenic soft X-ray tomography (Cryo-XT)*: The technique is based on atomic absorption and inherently offers high contrast at the nanoscale level. The Cryo-XT volume reconstruction (**b**) and surface rendering (**c**) clearly map the mid-trophozoite stage having a single large nucleus (Nu), digestive vacuole (DV) containing a large number of hemozoin crystals approximately aligned parallel to the inner membrane surface of the DV. This highlights the role of DV inner membrane surface as the common template for the hemozoin nucleation and crystal growth within an aqueous milieu. Alongside, hemoglobin transport vesicles (HTVs) are also seen; however, no presence of hemozoin crystals within HTVs or their path to DV is identified. Parts **b**, **c** of the figure are adapted with permission from ref. [46] Copyright: 2012, National Academy of Sciences.

hypothesized that deoxyHb withdraws an electron from the Fe^{2+} ion resulting in a low-spin Fe^{3+} ($S = 1/2$) state, and the oxygen is converted to superoxide O_2^- ($S = 1/2$), which is then taken into anti-ferromagnetic (AFM) exchange interaction.[54] Since healthy RBCs (h-RBCs) are primarily composed of oxyHb and contain a small amount of deoxy-Hb, healthy blood, also containing other diamagnetic components (water, white blood cells, etc.), collectively exhibits a negligibly weak diamagnetic/paramagnetic response (depending on the oxygenation).[55,56] Nevertheless, a measurable change in oxygen binding in many diseases like malaria,[55,57,58] diabetes mellitus,[59] methemoglobinemia,[60,61] sickle cell disease,[62] etc. results in a detectable change in the magnetic characteristics of human blood.

In 1946, M. Heidelberger and co-workers[63] used permanent magnets to separate malaria i-RBCs from blood plasma. This method relies on the magnetism of the malaria byproduct, hemozoin with Fe^{3+} (high-spin $S = 5/2$, paramagnetic) ions, as confirmed through electron spin resonance (ESR) and Mössbauer spectroscopy.[64,65] The efficiency of separating i-RBCs is further improved by the use of gradient magnetic fields,[66–68] known as magnetophoresis, and improvement in microfluidic channels [see

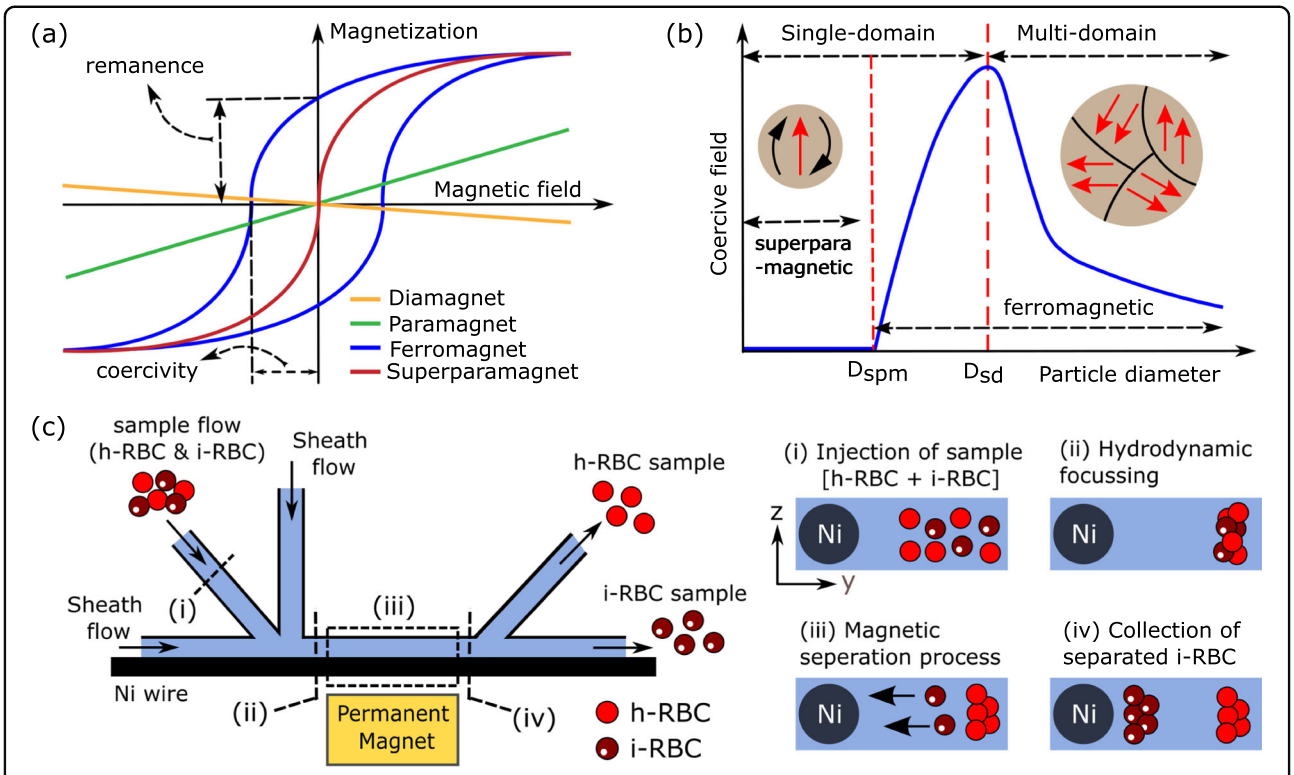

Fig. 3 Magnetism in nanocrystals and malaria-infected RBCs. a Magnetism in matter is governed by electron spin and orbital angular momentum (paramagnetism, PM) and external magnetic field-induced change in orbital motion (diamagnetism, DM). In an applied magnetic field, both attain a (proportional) cumulative moment, but once the external field is withdrawn, both retrace to the initial state. The non-interacting moments in PMs undergo a cooperative arrangement (under quantum-mechanical exchange interaction) below a critical temperature (T_C) with the emergence of domains having unidirectional spin arrangement (ferromagnet, FM), which retains a (remnant) magnetization even after the field removal. A reverse (coercive) magnetic field is required for demagnetization. **b** A reduction in particle size decreases the tendency of domain formation (and coercivity increases), whereas in a single-domain state (below D_{sd}), net magnetization (and coercivity) decreases and, below a limit (D_{spm}), typically in nanometers, the spins freely flip under thermal effect, and coercivity appears zero (if measurement time is greater than spin flipping time). Such nanomagnets are referred to as superparamagnets (SPM) having high (saturation) magnetization (similar to FMs), but no remanence (similar to PMs). **c** *Magnetophoresis*: The technique uses a magnetic force due to the high gradient magnetic field (e.g., by placing an FM in a uniform external magnetic field by permanent magnets) for migration of magnetic entities through a viscous medium. The cell tracking velocimetry further gives a single-cell magnetic susceptibility, making it a more effective and sensitive probe (than bulk magnetometry methods) for biological specimens (e.g., iron (Fe)-containing blood). The methodology was successfully employed for the separation and magnetometry of malaria-infected red blood cells (i-RBCs), employing the magnetic nature of malaria pigment, hemozoin. Part **c** of the figure is built upon the material adapted with permission from ref. [70] Copyright: 2013, American Chemical Society.

Fig. 3 for example].[20,69,70] The analysis of field-induced cell transport, termed magnetophoresis mobility (M.M.),[71] provides a quantification of the relative (w.r.t. medium) magnetic susceptibility ($\Delta\chi_V = \chi_{sample} - \chi_{medium}$) of live erythrocytes. This method revealed a negative $\Delta\chi_V$ (diamagnetic) for oxy-Hb, while a positive $\Delta\chi_V$ (paramagnetic) for deoxy-Hb and met-Hb[71] [see Table 2], thereby confirming the observations made by Pauling and Coryell.[52,53] The M.M. methodology has also demonstrated a graduated increase in $\Delta\chi_V$ for i-RBCs in malaria-developmental stages, with an increase in the hemoglobin-to-hemozoin conversion factor of up to 50% or more in the mature (schizont) stage.[57] The $\Delta\chi_V$ obtained from the M.M. method is validated by the bulk magnetometry method, which measures field-dependent magnetization (M-vs-H) for separated i-RBCs, as conducted by Hackett et al.[55] This study also examined isolated hemozoin crystals and obtained two orders of magnitude higher χ_V, which corresponds to an effective magnetic moment, $\mu_{eff} = 5.1\ \mu_B$/Fe, associated with high-spin Fe^{3+} (high-spin S = 5/2) in hemozoin.

To gain further insights into the magnetism of solitary hemozoin, its structural analog, lab-grown β-hematin nanocrystals[72,73] were investigated. In 2013, Butykai et al.[74] conducted a magnetometry study on randomly oriented crystals (in powder form) and magnetically aligned crystals in liquid suspensions (achieved through a freezing process in the presence of a magnetic field). They observed a significant difference in magnetization along the plane of the porphyrin rings (referred to as the

Table 2 The comparison of magnetic properties of blood corpuscle [with Fe spin state], healthy and malaria-infected RBCs in developmental stages [with different percentages of hemoglobin to hemozoin conversion], natural hemozoin, and its synthetic analog, *β*-hematin [with a specific crystal long-axis dimension, if defined], at room temperature.

Corpuscle	Method	Parameter	Value [SI]	Magnetism	Reference
Oxyhemoglobin [S = 0]	M.M.	$\Delta\chi_V$	-0.18×10^{-6}	DM	[71]
Deoxyhemoglobin [S = 2]	M.M.	$\Delta\chi_V$	3.3×10^{-6}	PM	[71]
Methemoglobin [S = 5/2]	M.M.	$\Delta\chi_V$	3.9×10^{-6}	PM	[71]
Healthy RBC	M-vs-H	$\Delta\chi_V$	$0.01(5)\times10^{-6}$	DM/PM	[55]
Infected RBC (ring) [15%]	M.M.	$\Delta\chi_V$	0.82×10^{-6}	PM	[57]
Infected RBC (trophozoite) [19%]	M.M.	$\Delta\chi_V$	0.91×10^{-6}	PM	[57]
Infected RBC (schizont) [50%]	M.M.	$\Delta\chi_V$	1.8×10^{-6}	PM	[57]
Infected RBC (gametocyte)	M.M.	$\Delta\chi_V$	200×10^{-6}	PM	[79]
Hemozoin	M-vs-H	χ_V	314×10^{-6}	PM	[55]
β-hematin	M-vs-H	χ_V	371×10^{-6}	PM	[55]
β-hematin (L = 200–300 nm)	M-vs-H	χ_V	3842	SPM	[78]
β-hematin (L = 1010 ± 340 nm)	M-vs-H	χ_V	374×10^{-6}	PM	[76]
β-hematin (L = 670 ± 280 nm)	M-vs-H	χ_V	387×10^{-6}	PM	[76]
β-hematin	M-vs-H	χ_V	410×10^{-6}	PM	[77]
Hemozoin	NV-ODMR	χ_V	340×10^{-6}	PM (≈95%)	[87]

For units' conversion, the density and molecular weight of *β*-hematin are taken as 1440 kg/m^3 and 633.5 g/mol, respectively. Abbreviations: *S* spin value, *L* long-axis dimension of the crystals, *M.M.* magnetophoretic mobility, *M-vs-H* field-dependent magnetization, *NV-ODMR* nitrogen-vacancy optically detected magnetic resonance, relative (with respect to medium) magnetic volume susceptibility, $\Delta\chi_V$ $\chi_{sample} - \chi_{medium}$, *DM* diamagnetic, *PM* paramagnetic, *SPM* superparamagnetic.

magnetic easy-plane, M_x) and its perpendicular C_{4v} rotation axis (referred to as the magnetic hard axis, M_z) with a ratio of $M_x/M_z \approx 9.6$ (at 2 K). This ratio decreased with increasing temperature but remained noteworthy at $M_x/M_z \approx 1.16$ at room temperature. These findings were consistent with an earlier multi-frequency high-field ESR study[65] on both hemozoin and β-hematin at cryogenic temperature (10 K). The ESR study used a spin Hamiltonian model with nearly axial symmetry, represented as $H = \mu_B \mathbf{g}\mathbf{S}.\mathbf{B} + D[S_z^2 - S(S+1)/3] + E(S_x^2 - S_y^2)$, which revealed a dominance of zero-field splitting (D) term associated with an axial anisotropy, with a negligible contribution from E-term, accounting distortion in C_{4v} symmetry (in porphyrin ring), as $|E/D| = 0.035$. The magnetic field-induced Zeeman-splitting yielded an almost isotropic g-factor ≈2. This ESR study,[65] supported by the findings of magnetometry study by Butykai et al.,[74] suggests hemozoin is a highly anisotropic easy-plane paramagnet.[75]

Though Butykai et al.[74] observed a linear M-vs-H (paramagnetic) behavior at room temperature, the low-temperature spectra obtained at 2 K, also measured by Gossuin et al.,[76] displayed a non-linear behavior with technical saturation, a characteristic associated with cooperative spin ordering, as in FM materials. In a big surprise, Inyushin et al. obtained a nearly saturated M-vs-H loop at room temperature, which exhibited zero remanence and coercivity, suggesting hemozoin is a superparamagnet (SPM). This observation is well supported by their theoretical ab initio calculations. SPM property is further validated by a significantly high magnetic susceptibility, $\chi_V \simeq 3842$, which is orders of magnitude greater than χ_V values reported in other studies on both natural and synthetic hemozoin [see Table 2]. Subsequently, Giacometti et al.[77] conducted a magnetometry study on β-hematin crystals obtained from the same manufacturer as those used by Inyushin et al.[78] This study observed a linear M-vs-H response under similar field conditions, indicative of a paramagnetic character at room temperature. In a nutshell, M.M. experiments[57,79] conducted on malaria-infected blood in a fixed applied magnetic field gives a susceptibility of the order of 10^{-6} [see Table 2], which falls within the range (usually $<10^{-3}$) associated with paramagnets. However, the typical confirmation of a paramagnet is a linear field-dependent magnetization, observed up to magnetic fields of a few tenths of Tesla. The majority of magnetometry studies put forward a paramagnetic behavior at room temperature,[55,74,76,77] with one notable exception showing SPM characteristics.[78] The significant distinction between the two scenarios lies in the notably smaller long axis of *β*-hematin crystals that exhibit SPM behavior [see Table 2].

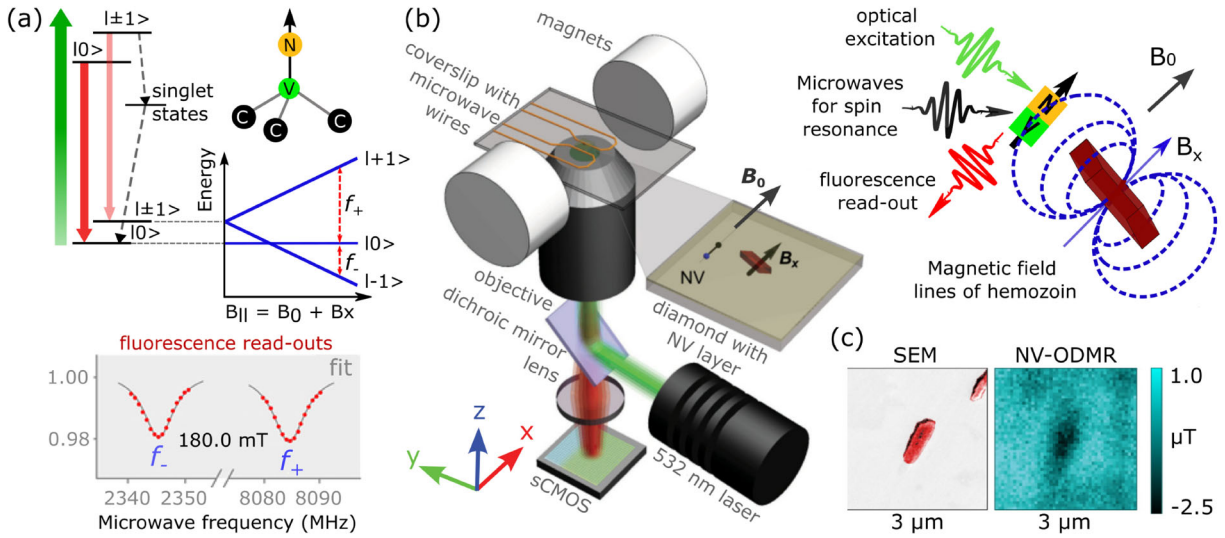

Fig. 4 Magnetic detection and mapping of individual hemozoin crystals by nitrogen-vacancy (NV)-based diamond quantum sensor. This exploits the magnetic resonance of spin associated with (fluorescent active) quantum defects, such as nitrogen-vacancy (NV) centers in diamond. The key feature that allows for magneto-optic sensing is the correlation between spin and fluorescence, resulting in two crucial consequences: (1) The radiative fluorescent intensity depends on the spin state, allowing for optical readout of the spin state, making it highly sensitive and suitable for super-resolution imaging. (2) Non-radiative processes allow spins to be polarized by orders of magnitude greater than those achieved by nuclear spins in high magnetic fields at room temperature through thermal polarization, the technique used in conventional magnetic resonance imaging (MRI) machines. These factors, along with a long spin-lifetime and the atomic nature of the NV defect, enable optically detected magnetic resonance (ODMR) of NV with an unparalleled combination of high sensitivity and spatial resolution, allowing for magnetic imaging of individual hemozoin nanocrystals. **a** Energy-level diagram (Field-frequency dispersion) of NV (spin-1) defect complex (a vacancy adjacent to substitutional nitrogen) in the diamond lattice. The ground state magnetic sublevel (±1) degeneracy is broken under the action of a magnetic field (we focus on fields parallel to NV axis, $B_{||}$), whether externally applied (B_0) or local (B_x) from the sample. Microwaves matching with $|0\rangle \leftrightarrow |\pm1\rangle$ spin transition frequencies ($f_{\pm}$) cause magnetic resonance, which is optically detected using spin-dependent fluorescence. In the experiment, a green laser excites the NV defect complex, and the resultant fluorescence intensity is measured, showing a sharp decrease at magnetic resonance frequencies ($f_{\pm}$), and their separation depicts the local magnetic field (B_x) from the Hemozoin nanocrystals. **b** An example of an epifluorescence setup for NV-ODMR, combining optical microscopy with a magnetic resonance set-up. A green laser induces red fluorescence in the diamond sample, which contains a thin layer of NV centers near the surface, placed on the coverslip. Hemozoin nanocrystals are situated on the diamond sample, in close proximity to the NV centers. A magnetic field oriented along one of the four possible NV axes is applied using permanent magnets. Microwaves are applied to the NVs via an antenna patterned on the coverslip. **c** An example of a magnetic image of a hemozoin nanocrystal constructed using NV-ODMR (right) compared with a scanned electron micrograph (left). The figure is built upon the material adapted with permission from ref. [87] Copyright 2019 American Physical Society (CC BY 4.0).

Indeed, SPM is a property associated with finite-size effects [see Fig. 3], a phenomenon encountered in widely studied magnetic nanomaterials.[80,81]

The bulk (superconducting quantum interference and vibrating sample) magnetometry[55,74,76,77] and magneto-phoresis mobility[57,79] experiments measure the (collective) magnetic susceptibility of hemozoin ensembles, encompassing a sizeable range of nanocrystal dimensions. This distribution in crystal size may play an important role in the magnetic ground state of hemozoin. To resolve this issue, magnetically-active optical defects, e.g., Nitrogen-Vacancy (NV) centers in diamond,[82–84] offer high sensitivity at a nanoscale spatial resolution to individually identify FM and SPM particles.[85,86] Fescenko et al.[87] employed an NV-based diamond quantum sensor to measure the stray magnetic fields produced by individual hemozoin crystals when subjected to external magnetic fields [see Fig. 4]. This study revealed a paramagnetic response with $\chi_V \simeq 340 \times 10^{-6}$, consistent with the findings from the bulk magnetometry study,[55] for over 95% nanocrystals (with a long axis >200 nm). On the contrary, the smaller nanocrystals exhibited higher magnetization, following a Langevin field dependence, characteristic of SPM behavior, thus supporting the bulk magnetometry study on β-hematin crystals conducted by Inyushin et al.[78] It is worth noting that, as crystal size increases, a transition from SPM to FM regime is commonly observed in magnetic nanomaterials[80,81] [see Fig. 3]. Nevertheless, NV-ODMR imaging of individual hemozoin crystals highlights the crucial role of crystal morphology in determining the magnetic properties of hemozoin. The origin of this peculiar SPM nature/impurity in smaller nanocrystals holds significance in understanding the hemozoin formation in the early ring stage of malaria.

Hemozoin sensing technologies

Magnetic-based technology

The magnetism in malaria-infected erythrocytes, associated with hemozoin, is firstly employed in the magnetophoretic method, as discussed in Section "Magnetism of hemozoin: a double-edged sword", which serves as an effective tool for magnetic characterization of biological fluids. Jeonghun Nam et al.[70] successfully separated i-RBCs from h-RBCs through microfluidic channels, achieving a recovery of 73% for early-stage (ring) i-RBCs and over 98% for late-stage (trophozoites and schizonts) [see Fig. 3]. This approach has also offered an initial step in concentrating i-RBCs for improved diagnostic performance using existing methodologies.[88,89] Conventional light microscopy is limited due to the time-consuming nature of optical scanning, which involves visually scanning the entire slide. However, magnetic enrichment, as seen in magnetic deposition microscopy,[88] enhances the ability to visualize i-RBCs at specific positions, making staining and scanning more efficient and reducing the time required for diagnostics. This approach has been demonstrated for all the human malaria parasite species, with at least a 40-fold enrichment for *P. falciparum* and up to a 375-fold enrichment for *Plasmodium ovale* infections, significantly enhancing sensitivity compared to conventional light microscopy. Furthermore, a microfluidic device, incorporating coupled magnetic beads (for capturing i-RBCs) and quantum dot-antibodies conjugates (for detecting *P. falciparum* secreted HRPII), has been reported.[89] This device enables quantitative immunoassay assessment with at least a 10-fold increase in sensitivity compared to traditional RDTs. Therefore, magnetic enrichment offers new possibilities for enhancing existing clinical malaria diagnostic methods.

The idea of magnetism in hemozoin in recent history was examined in nuclear magnetic resonance (NMR) relaxometry studies.[17,90,91] The relatively large magnetic susceptibility of these hemozoin crystals induces substantial changes in the transverse relaxation rate of proton NMR in RBCs to infer the 'parasite load' in blood. This idea was initially reported by Karl et al.[92] The team, however, concluded that NMR relaxometry (using unprocessed raw blood) was unlikely to have enough sensitivity for malaria diagnosis in the field setting. Weng Kung Peng and co-workers[58,93,94] demonstrated that it was possible to have an ultrasensitive malaria diagnosis by increasing the filling factor of the probe and introducing a vital enrichment step to separate the i-RBCs from h-RBCs via hematocrit centrifugation. This breakthrough was observed with a portable benchtop micro-NMR system utilizing an ultra-short echo technique (UET) [see Fig. 5a–c] in their in vitro cultured *P. falciparum* parasites as well as in vivo mice studies, demonstrating rapid (less than 5 min) and ultrasensitive detection (<10 parasites/μL) for the early-stage malaria infections. The minimal sample processing steps (without any chemical or immunolabeling) reduce human-induced errors for measurements in the field setting. Subsequent to this development, several similar works were reported,[95] introducing new functionalities to enhance i-RBCs separation (using microfluidic margination[96] and lysis control[97]). NMR relaxometry has also been employed for drug studies.[98]

The process of hemozoin formation is mediated heavily by the transfer of an electron. The use of higher dimensional NMR or ESR spectroscopy (or a combination of them)[99] should have the capability to differentiate the detailed structure of hemozoin, enabling the identification of Plasmodium species. In a related development, in 2020, Weng Kung and his team[59] demonstrated the use of (pseudo) two-dimensionality (2D) in the time-domain NMR to obtain highly specific and unique molecular fingerprinting of various redox (and hence oxidative/nitrosative) states of hemoglobin from a single drop of blood [see Fig. 5d–g]. This T_1–T_2 relaxometry approach (termed as 'Clustering NMR'[100]) may be extremely useful for rapid and accurate object classification using a low-field micro-NMR system. This new methodology is demonstrated in the clinical point-of-care diagnosis of diabetes based on the oxidative status of blood.[59]

Another way of recording weak magnetic fields is based on spintronics, utilizing the spin-related magnetoresistance effect, which is the tendency of a material (often ferromagnetic) to change its electrical resistance as a function of the magnitude and direction of the applied magnetic field. This phenomenon has led to the development of giant magnetoresistance (GMR) and tunneling magnetoresistance (TMR) sensors, borrowed from advanced technology in hard disc drives and high-density magnetic memory. Now, it is tackling the next generation of ultrasensitive magnetic sensors for detecting low pico-Tesla level magnetic fields. Recently, Heidari and his team[101] demonstrated a proof-of-principle for a miniaturized, low noise, low power, and highly sensitive TMR sensor using a CMOS analog front-end readout circuit for the detection of paramagnetic hemozoin nanocrystals [see Fig. 6a–e]. The team has developed the first miniaturized and handheld TMR-based device with the following components: a sensor, a handheld permanent magnet for magnetizing of the hemozoin crystallites, and an analog front-end circuitry for signal amplification and noise cancelation, which can all be integrated into an easily portable compact and cost-effective design. This magnetic-based lab-on-chip platform potentially offers a rapid and easy-to-use malaria diagnostic method without direct contact of blood samples via excellent compatibility with electronic devices.

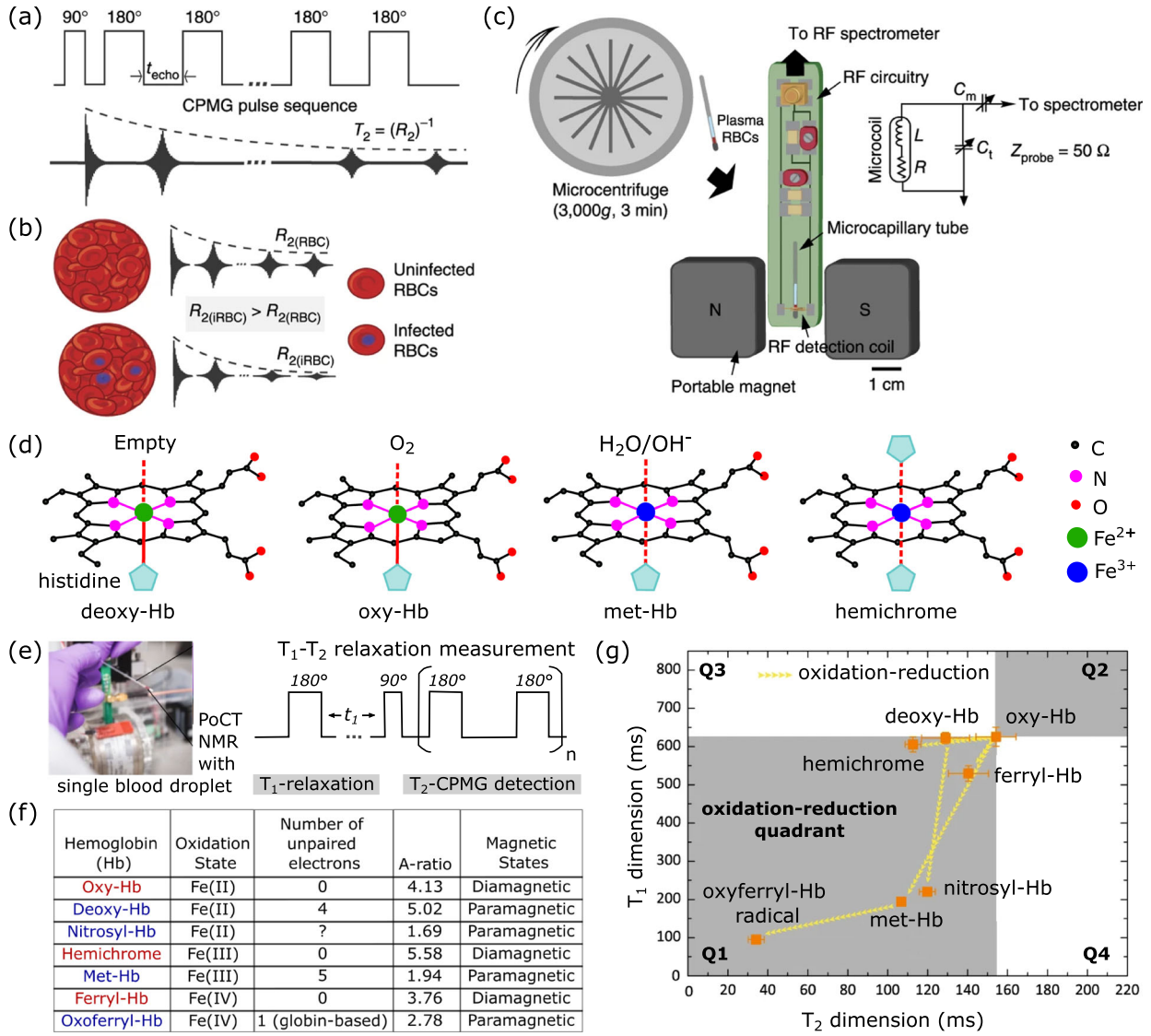

Hemoglobin (Hb)	Oxidation State	Number of unpaired electrons	A-ratio	Magnetic States
Oxy-Hb	Fe(II)	0	4.13	Diamagnetic
Deoxy-Hb	Fe(II)	4	5.02	Paramagnetic
Nitrosyl-Hb	Fe(II)	?	1.69	Paramagnetic
Hemichrome	Fe(III)	0	5.58	Diamagnetic
Met-Hb	Fe(III)	5	1.94	Paramagnetic
Ferryl-Hb	Fe(IV)	0	3.76	Diamagnetic
Oxoferryl-Hb	Fe(IV)	1 (globin-based)	2.78	Paramagnetic

Fig. 5 Micro nuclear magnetic resonance (NMR) relaxometry for rapid and early-stage malaria diagnostics. a The technique inspects the (^{1}H) proton nuclei spin dynamics by applying radio-frequency (RF) pulses at resonance frequency (corresponding to Zeeman splitting in a fixed external magnetic field) in the Carr–Purcell–Meiboom–Gill (CPMG) sequence. Over thousands of echoes, the signal decay rate, R_2 (= $1/T_2$, transverse relaxation time), is measured. **b** In the presence of hemozoin (with a large relative magnetic susceptibility) in i-RBCs, the T_2 for proton nuclei spins decreases substantially compared to those in healthy RBCs, such that $R_{2(iRBCs)} > R_{2(RBCs)}$. The change in R_2 provides a quantification of parasitemia level (%). **c** The benchtop micro-NMR system uses a permanent magnet, home-built radio-frequency (RF) detection probe connected to an RF spectrometer, which serves as a transmitter and receiver of the RF signal. The setup is examined with highly-synchronized "ring-stage" i-RBCs (to a limit of fewer than 10 parasites/μL) after magnetic separation of later (trophozoite and schizont) states i-RBCs, followed by removal of remaining h-RBCs in a blood sample through hematocrit centrifugation in a microcapillary tube. The whole diagnostic process for *P. falciparum* is demonstrated within 5 min. Redox states of hemoglobin: **d** In the non-protein part of hemoglobin, i.e., heme, Fe has six co-ordination sites with four attached to the porphyrin (nitrogen) ring and one to histidine (globin chains), leaving (sixth) one site free for bonding, responsible for oxygen transport in our body. The most common hemoglobin species are shown here with the (sixth) empty site (deoxy-Hb), bonded with oxygen (oxy-Hb), H_2O or OH^- (met-Hb), and histidine (hemichrome). This bonding decides the Fe valence states (and thus, spin states) and magnetism in blood. (Pseudo) two-dimensional (2D) T_1–T_2 magnetic spectroscopy: **e**, **f** Various redox states of Hb are evaluated by measuring water proton spin relaxations in newly proposed (pseudo) two-dimensionality (longitudinal, T_1 and transverse, T_2) by point-of-care technology (PoCT) micro-NMR system using a single drop of blood. The technique employs standard inversion recovery (for T_1) and CPMG (for T_2) rf pulse sequences in an array of echoes (a few thousand) to obtain a high signal-to-noise ratio. In biochemical processes (e.g., oxidation, nitration), Fe oxidation states (e.g., Fe^{2+}, Fe^{3+}) in hemoglobin and its environment are induced for controlled oxidative stress, which introduces a subtle change in the (predominantly) bulk water molecular environment (because of its property of forming hydrogen bonds with most macromolecules), resulting in a measurable sensitivity to water proton nuclei spin dynamics (relaxometry). **g** Each hemoglobin species (with respective Fe oxidation states and molecular environment) occupies a unique space in the T_1–T_2 relaxometry coordinate system. Simultaneous T_1–T_2 relaxometry measurements (with slight modification in rf pulse sequences) result in more accurate object identification than relying on only one (T_2). The figure is built upon material adapted with permission from the author (W. K. Peng) previous studies, ref. [58] Copyright: 2014, Nature Publishing Group and ref. [59] Copyright 2020 Springer Nature (CC BY 4.0).

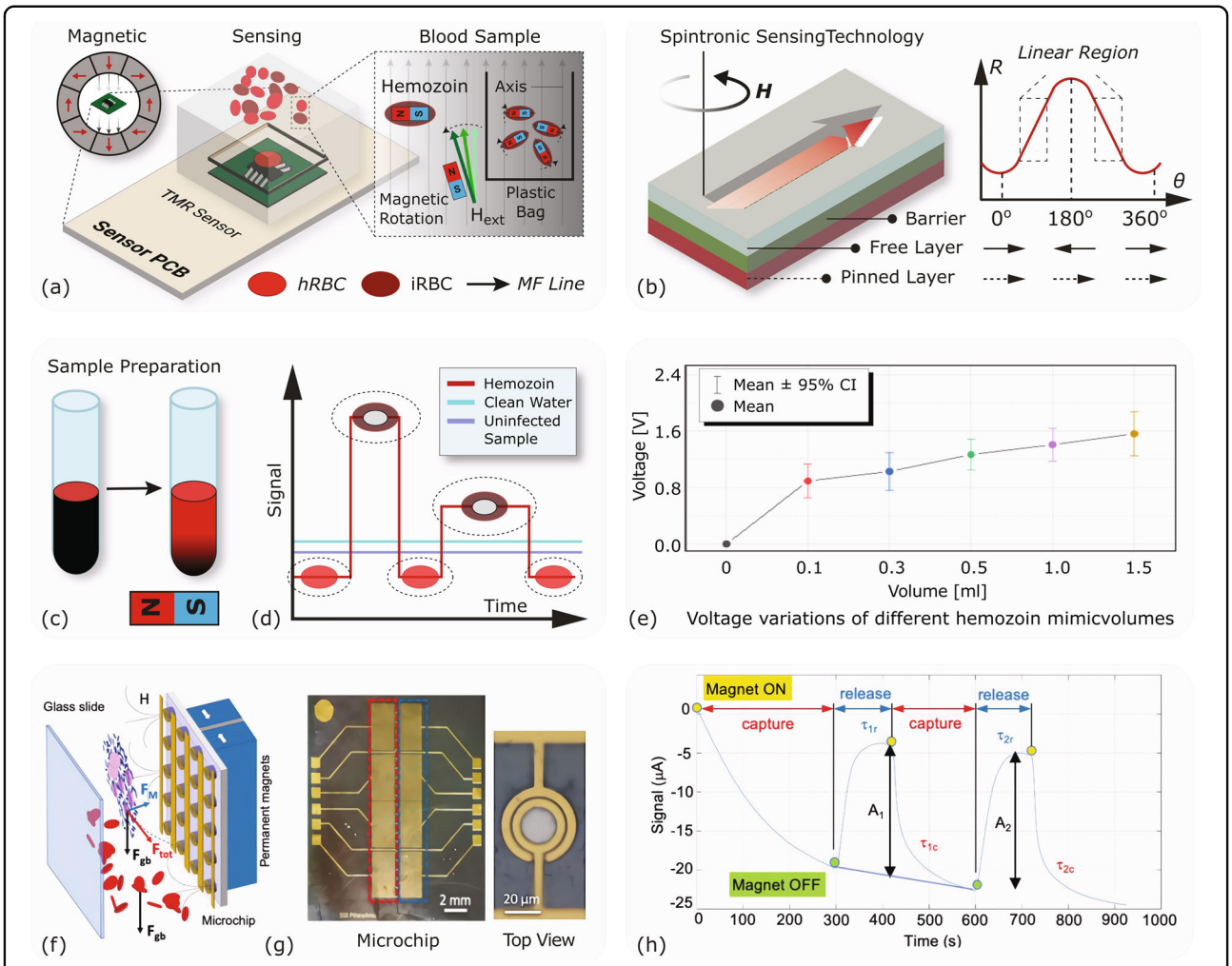

Fig. 6 Lab-on-chip tunnel magnetoresistance (TMR) and TMek sensor for malaria diagnostics. a A handheld magnetic-based lab-on-chip sensing platform, including TMR sensor, magnet, Halbach array, analog front-end (AFE), and printed circuit board (PCB). Red arrows represent the magnetization directions of individual magnets, and MF is the magnetic field lines generated by the Halbach array. A portable magnet is entailed to magnetize hemozoin crystals inside the i-RBCs. **b** The basic structure and transfer curve of the TMR sensor. **c** Sample preparation with disposable pouches fitted or a tube. **d** Measured signals from hemozoin of the i-RBCs, compared to h-RBCs and clean water. **e** Voltage variations of different hemozoin mimic volumes. **f** A sketch of the TMek magnetophoretic separation process. Two external NdFeB magnets with north poles facing each other generate high field gradients around the Ni concentrators to capture i-RBCs (pink) and hemozoin crystals (black), while the rest, h-RBCs, are sedimented under gravity. **g** The left panel shows a picture of a microchip with the measurement (red) and reference (blue) areas, while the right panel highlights the top view of the annular gold (measurement) electrodes on top of Ni concentrators (the reference electrodes are placed nearby, without concentrators). Two counter phase voltage signals (at 1 MHz) are applied to the outer rings, while the inner ones are connected to the virtual ground of transimpedance amplifier (TIA). When i-RBCs (and hemozoin crystals) are captured on the measurement side, the impedance changes, and a net differential current flows into the TIA. **h** Measured current signals for a couple of measurement cycles where the magnet assembly is brought closer (Capture Phase) and taken away (release phase). The amplitude and shape of the waveform during the release phase contain information about the hemozoin concentration (parasitemia) and the stage of the malaria infection, respectively. With a capture time of 10 min, the techniques can detect as low as 10 parasites/µL within the whole process in 20 min. This figure is adapted with permission from (**a**–**e**) ref. [101] Copyright: 2021, IEEE Publishing Group and (**f**–**h**) ref. [79] Copyright 2021 Wiley-VCH (CC BY 4.0).

Towards another lab-on-chip diagnostic technology, R. Bertacco and co-workers[79,102] have developed a microchip-based diagnostic tool, namely TMek, which relies on the magnetophoretic separation of magnetic malaria corpuscles, and the measurement of impedance variation caused by these corpuscules [see Fig. 6f–h]. The team utilized micro magnetic concentrators to create a high magnetic field gradient, effectively competing with gravity to separate i-RBCs (containing hemozoin crystals) at localized sites within a silicon microchip (for a fixed capture time), where a highly sensitive electrical detection is performed. Upon taking magnets away (release phase), the amplitude of variation in the signal provides a quantification of the parasitemia level. Additionally, the time

evolution of the electrical signal (waveform) exhibits distinctive patterns corresponding to different malaria infection stages. This single microchip, without the need for active microfluidics, can quantify parasitemia at concentrations as low as 10 parasites/μL, offering the potential for a stage-selective malaria diagnosis.

Optical-based technology

Alongside its peculiar magnetic properties, hemozoin exhibits rich optical characteristics, including high optical absorbance,[103] birefringence,[104] and nonlinear dielectric susceptibility,[105] among others, which provide opportunities for optical quantification of malaria parasites.

In a straightforward approach, light absorbance was measured in vivo in a mice study;[106] however, the sensitivity (>0.03%) is insignificant for early diagnosis. More recently, Susana O. Catarino and co-workers exploited optical spectrophotometry in both absorbance[103] and reflectance[107] modes. In the absorbance mode, the team successfully detected synthetic hemozoin in healthy blood down to a limit of 1 μg/mL with high specificity, while in reflectance mode, they achieved the detection of *P. falciparum* parasites at concentrations as low as 12 parasites/μL, using thin-film optical filters.

The birefringent property of hemozoin, which induces depolarization of light at 90° relative to the laser, was harnessed through polarization microscopy[104] within the sensitivity range of light microscopy. Hemozoin birefringence has also been employed in automated flow cytometry, with commercial Cell-Dyn analyzers.[108] However, the high cost and the bulky setups limit their widespread use in resource-poor settings.[109] The integration of photoacoustics into flow cytometry allows for in vivo ultrasensitivity of 0.005 parasites/μL,[110] but this requires a high dilution (to the extent of one cell under laser irradiation) and, consequently, long processing times (in hours). This processing time is significantly reduced to just a few minutes with the use of a surface-acoustic-wave (SAW) sensor.[111,112] However, this approach is currently demonstrated for a limited sensitivity of ring-stage 0.5% parasitemia in the whole blood. The team intends to increase the sensitivity by integrating this SAW sensor into a proposed optoacoustic microfluidic device.[113] Moreover, Pourabed et al.[114] have recently developed an acoustically actuated microfluidic mixer for enhancing whole blood lysis in just 2 s. This platform, when combined with a spectroscopic approach, holds the potential for rapid malaria diagnostics using whole blood samples.

The optical properties of hemozoin have also been explored under the action of ultrashort near-infrared (NIR) laser pulses, leading to the formation of transient vapor nanobubbles around hemozoin[115] and efficient third-harmonic generation (THG).[105,116] These hemozoin-induced vapor nanobubbles (H-VNBs) were detected using a photoacoustic probe in a mice study down to 0.0034% (≃17 parasites/μL) in seconds in a non-invasive manner. In human blood, detection has been extended to even lower parasitemia levels, reaching 0.0001% (≃5 parasites/μL). On the other hand, THG imaging of hemozoin[105,117] in a scanning cytometry approach[116] can provide single-cell characterization in an automated and rapid scanning process that takes just a few minutes. This methodology was validated with blood samples obtained from malaria patients with parasitemia levels of 0.2% or higher, showing close consistency with light microscopy results. Although the two methods offer highly sensitive and rapid diagnostics, the initial requirement of expensive ultrashort laser sources presents a challenge for clinical diagnostics.

Vibrational (Raman and infrared) spectroscopy techniques [see Fig. 7] have emerged as powerful tools for extracting biochemical information and enabling low-cost clinical diagnostics for various diseases, including malaria.[22] Raman spectroscopy measures the characteristic (emitted) light wavelength from inelastic scattering by the hemozoin molecule.[118] However, the spontaneous Raman cross-section is typically weak, making it unsuitable for early diagnosis. This can be enhanced by matching the laser wavelength to electronic transitions, known as resonance Raman scattering (RRS), of hemozoin.[119,120] Remarkably, the total symmetric A_{1g} modes are very intense for hemozoin (compared to hematin) when applying near-infrared excitation wavelengths.[118] This enhancement may be attributed to excitonic interactions between aggregated porphyrin complexes at long excitation wavelengths. Another contribution comes from a broad z-polarized charge transfer transition that is centered at 860 nm, which is not observed in hemin or hematin.[119] Furthermore, the coupling of Raman spectroscopy with partial dark-field effect,[121] acoustic levitation,[122] and external magnetic field[123] has led to improved diagnostic capabilities. These advancements, however, are still not sufficient for early diagnosis of 'ring' stage infections.

A pronounced enhancement in the Raman signal is often achieved by leveraging the surface plasmon field of metallic nanostructures in contact (substrate), a technique known as surface-enhanced Raman spectroscopy (SERS).[124] Using gold-coated *G. Weskei* butterfly wings as a substrate, Garrett et al. achieved high sensitivity (25 parasites/μL) in 'ring' stage infected cells.[125] However, random hemozoin deposition and its tendency to form aggregates at the base of the conical wing nano-structures pose challenges in locating hot spots for detecting low parasitemia. Furthermore, hemozoin aggregation itself enhances the Raman peak intensity, making it unsuitable for accurately quantifying parasitemia. Moreover, common SERS substrates, such as silver nanoparticles

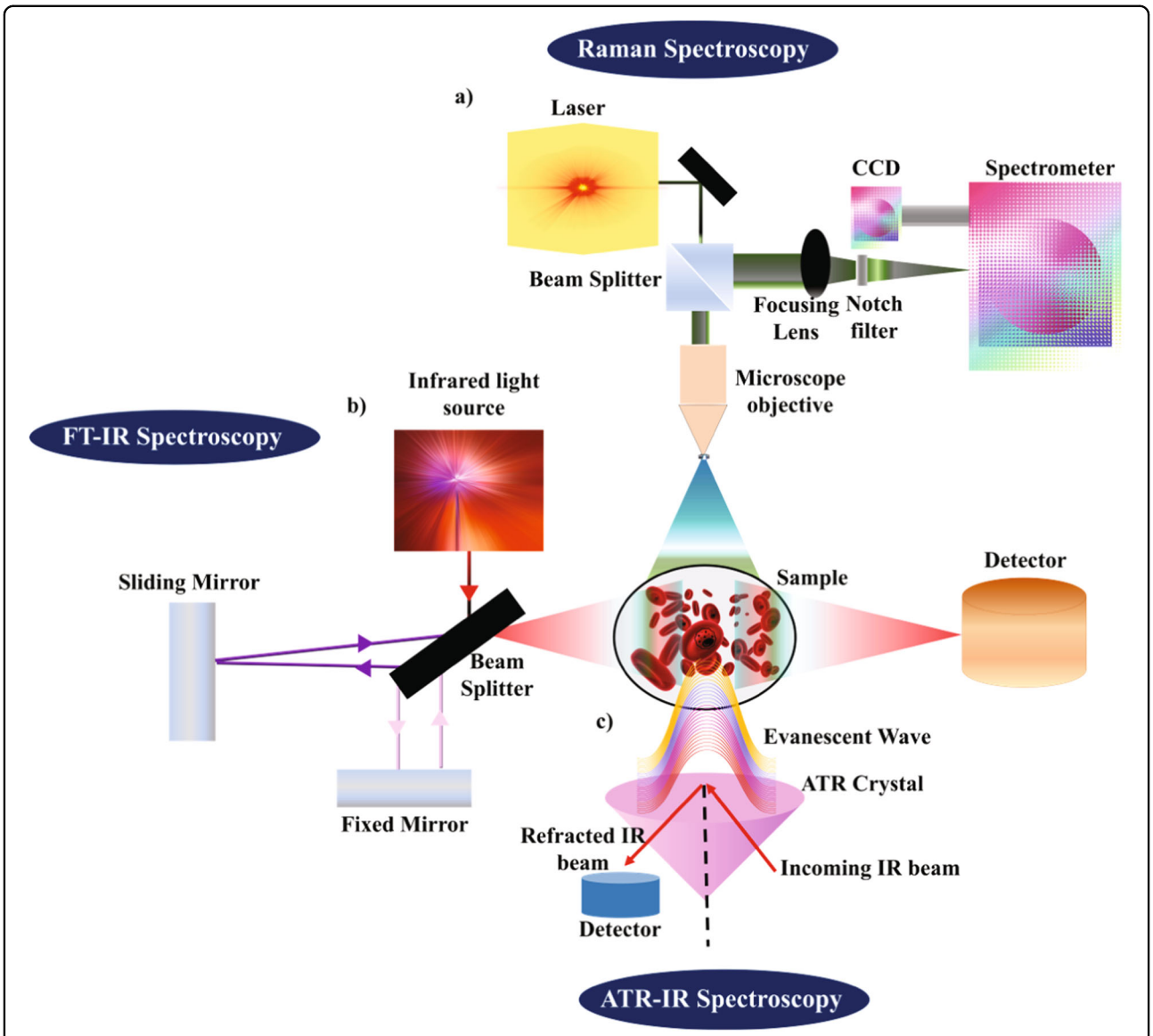

Fig. 7 Schematic of Raman and (Fourier transform and attenuated total reflectance) Infrared Spectroscopy. a In Raman spectroscopy, monochromatic radiation from a laser source, via a beam splitter and bandpass filters, is focused on the sample using a microscope objective. Inelastic interaction of illuminated light with molecular vibrations in the sample results in the emission of (Raman) characteristic light wavelengths, which are guided, via a combination of notch filter and grating monochromator, to a sensitive photon detector (generally, charge-coupled device) and used to construct a Raman spectrum. **b** In Fourier transform Infrared Spectroscopy (FTIR), a broadband infrared source beam is divided into two optical beams, which are directed to a fixed mirror and a second sliding mirror that moves with a constant velocity. Two reflected beams from the respective mirrors are recombined, now with a path difference, to construct an interference pattern (or interferogram). This is then sent to the sample, and the transmitted portion is measured with a detector, containing information on each infrared frequency (as a function of the sliding mirror position). **c** In Attenuated total reflectance (ATR) spectroscopy, an infrared beam is passed through the internal reflection element (i.e., ATR crystal), resulting in an evanescent wave (due to the contact with the specimen having a distinct index of refraction) that penetrates the sample (typically to a few microns) in contact with the ATR crystal. After undergoing a number of internal reflections, this wave exits the opposite end (of the crystal) and enters the detector to generate an infrared spectrum.

(AgNPs),[126] provided low sensitivity of 500 parasites/μL, but hemozoin aggregation using a core–shell magnetic Fe_3O_4@AgNPs in an external magnetic field enhances the sensitivity to 5 nM of β-hematin, equivalent to 30 parasites/μL.[123] Another approach involved the in situ synthesis of AgNPs inside Plasmodium parasites, reducing the substrate-hemozoin distance and yielding a sensitivity of 2.5 parasites/μL.[126] However, the chemical precursors used in this approach tend to convert hemoglobin (in uninfected h-RBCs in the blood) into heme and further

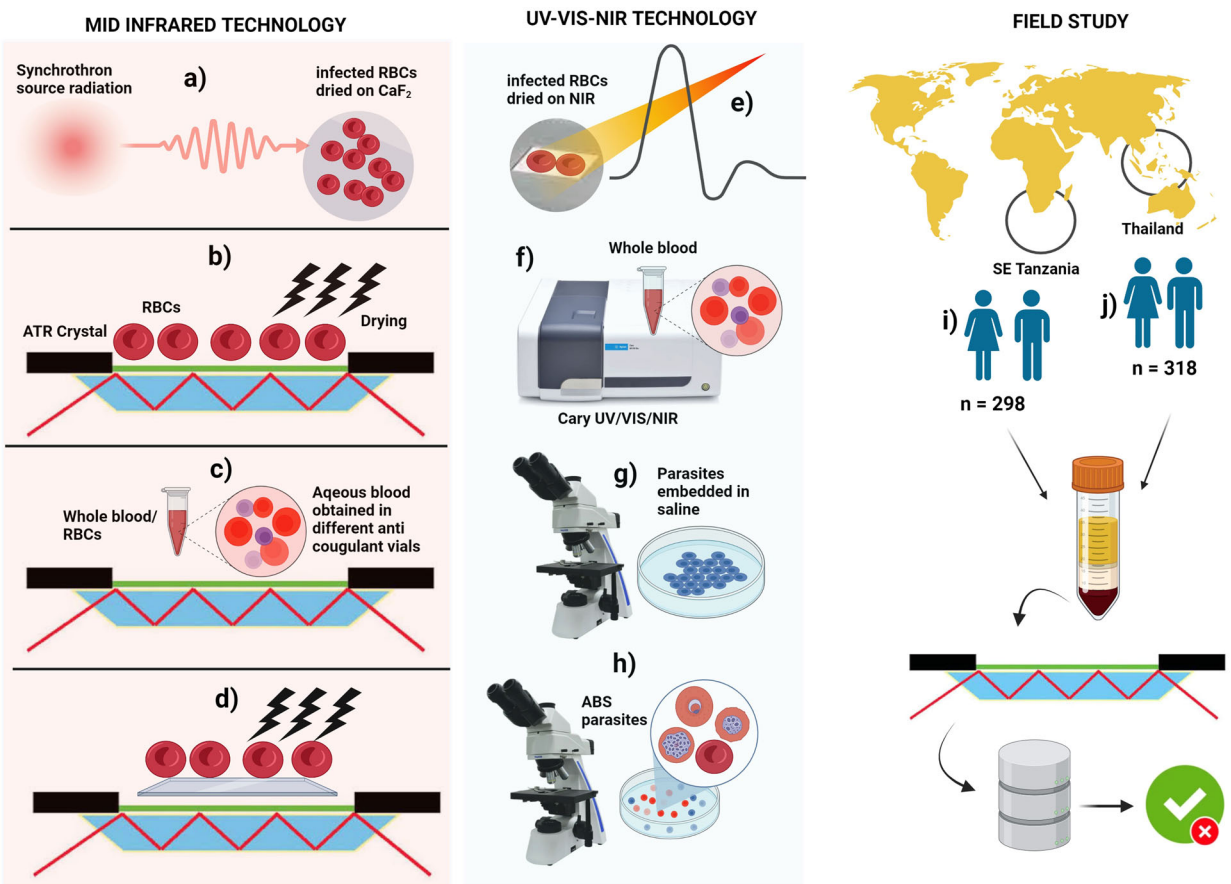

Fig. 8 Research summary of malaria diagnostic with ATR–FTIR, Ultraviolet(UV)–visible and near-infrared (NIR) spectroscopy. a–d The major research performed using mid-infrared spectroscopy for malaria detection and quantification. **a** Discrimination of intraerythrocytic life cycle stages of the malaria parasite using a synchrotron source FTIR.[130] **b** Detection and quantification of early-stage malaria infection using ATR-FTIR spectroscopy in isolated RBCs.[134] **c** Effect of common anticoagulants on quantification of malaria infection in aqueous whole blood.[136] **d** comparative study between a disposable coverslip and conventional optical microscopy glass substrate for mid-infrared spectroscopic studies. **e**, **f** The recent developments in malaria detection and quantification using UV–visible–NIR techniques. **e** First detection of *P. falciparum* parasites in dried red blood cells using a miniaturized NIR spectrometer.[170] **f** Comparative study of malaria detection with UV–visible and NIR spectrometer individually (and a combination of them) using fresh aqueous blood samples.[171] **g** Discrimination of the various asexual blood stages of *P. falciparum* at single cell levels in functional erythrocytes using visible microspectrophotometry.[172] **h** Interpretation of the ultraviolet–visible spectra of the malaria parasite *P. falciparum*.[193] **i**, **j** Field trials in malaria-endemic regions using portable ATR–FTIR spectrometers. The trials were carried out in **i** South Tanzania[156] using blood samples dried directly on a filter paper and **j** Thailand[155] using centrifugation of whole blood samples to obtain blood cells samples which were subsequently dried directly on the ATR crystals.

hematin, which has identical Raman peaks as hemozoin under visible light excitation[127]), potentially leading to false interpretations. To address this challenge, an extension of the excitation wavelength from visible light to near-infrared can enable the differentiation of the spectra of hemozoin and hematin. In an effort to develop a point-of-care test, the team applied an in situ AgNPs synthesis approach to a SERS fluidic chip, which, however, resulted in a reduced sensitivity of 125 parasites/μL in the ring stage.[128] In a recent SERS study employing gold nanostructures (AuNS),[129] a high sensitivity of 0.1 *P. falciparum* parasites/μL was achieved, allowing for accurate diagnosis of 25 clinical samples from *P. falciparum*- and *P. vivax*-infected patients and healthy volunteers. However, this process requires a significant amount of time (30 min).

Another basic optical tool for material identification is Fourier transform infrared spectroscopy (FTIR). Slater et al.[34] were the first to employ FTIR spectroscopy on purified hemozoin, identifying the presence of an iron carboxylate bond that links the heme units, forming dimers [see Fig. 2]. The distinctive hemozoin bands provide an excellent marker for developing an infrared-based diagnostic tool for malaria. This idea has been extensively explored by Bayden Wood and co-workers [see Fig. 8]. The team, initially, performed an infrared experiment on

RBCs fixed onto a CaF_2 substrate using synchrotron FTIR microspectroscopy and an artificial neural network to develop a diagnostic model.[130] Principal component analysis (PCA) revealed distinct hemozoin bands as the parasite metamorphosed, enabling discrimination of intra-erythrocytic life-cycle stages. By coupling a synchrotron light source with a focal plane array (FPA) infrared microscope system, they were able to discriminate single i-RBCs within a field of uninfected cells.[131]

In another development, the team spatially resolved sub-cellular parasite organelles on a conventional and affordable 'glass' slide using a high-resolution FTIR imaging spectrometer (Agilent Technologies, Inc.), combined with an automated approach based on Partial Least Squares-Discriminant Analysis (PLS-DA).[132] In another study,[133] the team applied a combination of Atomic Force Microscopy infrared (AFM-IR) and Raman spectroscopy to probe the localization of subcellular components within P. falciparum-infected RBCs using hyperspectral multimodal imaging. These merged images offer much more valuable information compared to individual modalities, providing a more comprehensive understanding of the cell composition and resulting in improved model predictions. However, these mid-IR techniques[130–133] are not suited as routine diagnostic tools.

In a laboratory setting, Wood and co-workers[134] demonstrated the potential of Attenuated Total Reflectance (ATR)-FTIR spectroscopy, in combination with multivariate data analysis tools, for a rapid (<3 min) malaria diagnosis (and quantification) with the required ease of sample preparation and high sensitivity. The absolute detection limit was found to be <1 parasite/μL for cultured early 'ring' stage parasites. It is noted that biochemical parameters, including lower levels of glucose, high levels of urea, and metabolic changes produced by the Plasmodium spp. could interfere in the prediction of clinical parameters and vice versa. To resolve this, the aforementioned methodology was successfully applied to diagnose malaria, glucose, and urea simultaneously from a single ATR-FTIR spectrum recorded from a drop of blood.[135] In order to eliminate the problematic RBCs fixing and drying steps, Martin et al. applied ATR–FTIR to aqueous physiological blood samples (including strongly IR-absorbent plasma, and water) under the action of three common anticoagulants: sodium citrate, potassium EDTA and lithium heparin.[136] PCA models built using aqueous physiological samples showed less influence from anticoagulants compared to the dried samples, presumably due to a dilution of anticoagulants by water. PLS-regression analysis (PLS-RA) indicated that only heparin individually gave the best prediction capability for low parasitemia (<0.1%).

Magneto-optical based technology

Malaria-infected blood containing hemozoin nanocrystals can truly be considered a magnetic fluid. An external magnetic field exerts a torque on hemozoin (elongated) crystals, aligning them unidirectionally such that the hard magnetic axis (at ~60° to the crystallographic long-axis[74]) lies normal to the field. As a result, hemozoin exhibits a preferred direction of optical absorption (optical anisotropy) under the action of linearly polarized light (optical dichroism).[137] This is analogous to the Cotton-Mouton effect, which is the birefringence of magnetic fluids in a transverse magnetic field. Thus, the magnetic anisotropy of hemozoin gives rise to optical dichroism, termed magnetically-induced linear dichroism (MLD), and hemozoin crystals behave like a dichroic polarizer.[74,137]

Newman and co-workers[138] first developed a simple magneto-optical diagnostic (MOD) tool that measures the difference in optical transmission through a fluid (e.g., blood) medium in zero and a constant applied magnetic field (0.6 T) with randomly oriented and magnetically aligned hemozoin crystals, respectively. The portable device can detect a concentration of hemozoin in blood as low as 5 ng/μL, notably in a quick turnaround time of 1 min. This development was followed by a similar portable device called Gazelle,[139] which exhibited a diagnostic capacity of ≥50 parasites/μL for *P. falciparum* within 1 min. Another portable optical diagnostic system (PODS)[140] brings a magnet close to the sample, thus pulling β-hematin out of the optical path, resulting in higher transmitted intensity. The difference between the two signals (magnets close and away) can detect β-hematin concentrations as low as 8.1 ng/mL in whole rabbit blood; however, the diagnosis takes a somewhat longer time of 10 min.

Newman and co-workers also exploited the MLD of hemozoin using polarization modulation of the laser beam in two orthogonal (parallel and perpendicular) directions with respect to the (fixed) magnetic field direction.[137] The proof of principle was demonstrated for a detection of less than 1 μg/mL concentration of β-hematin in whole fresh blood and more notably, hemozoin within live parasitized cells, promising an in vivo (non-invasive) diagnostic. Indeed, simulations on MLD of hemozoin in a medium resembling fingertip physiology indicated a detection capability of less than 0.02 μg/mL (equivalent to ≈33 parasites/μL) in a non-invasive methodology within a minute.[141]

In a similar MLD-based diagnosis, Butykai et al.[74] measured the polarization modulation of the (transmitted) light beam by magnetically driven rotation of (dichroic) hemozoin crystals, thus termed as rotating-crystal MOD (RMOD) technology [see Fig. 9a]. The light wavelength & magnet rotation frequency are optimized for the best signal-to-noise ratio for the detection of

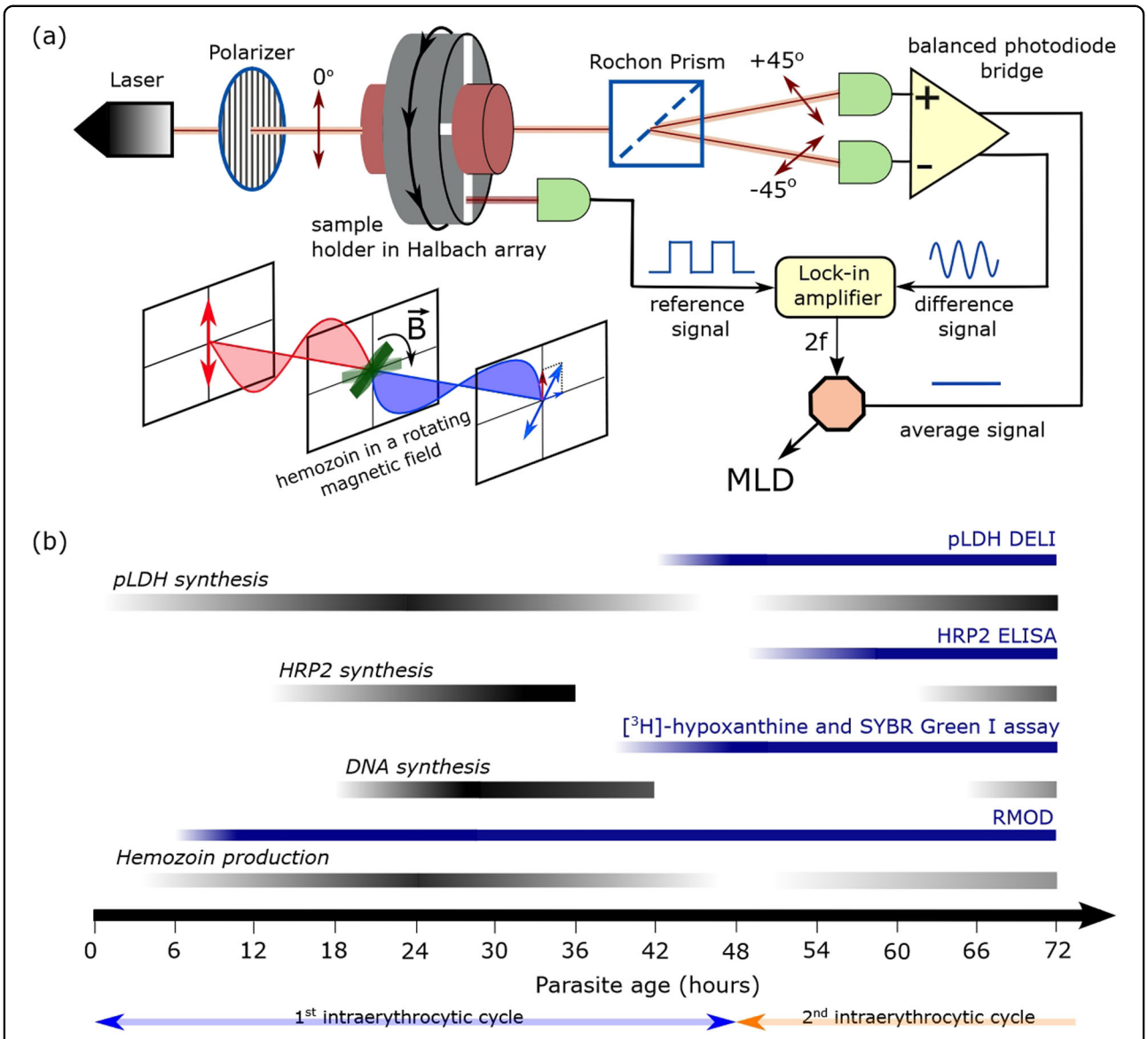

Fig. 9 Magnetically induced linear dichroism (MLD) of hemozoin for malaria diagnostics and antimalarial drug efficacy testing. a The (elongated) hemozoin suspended in a liquid medium can be magnetically oriented along its (magnetic) easy axis i.e., porphyrin plane. A magneto-optical setup measures the transmission of polarized light through a hemozoin-containing blood sample while the external magnetic field is rotated within a plane perpendicular to the direction of light propagation. This magnetically induced rotation of hemozoin dictates their optical anisotropy. To exploit this, the transmitted light is split into two orthogonal light polarizations (parallel and perpendicular to the magnetic easy axis), and their difference, known as magnetically induced linear dichroism (MLD), is measured. The signal-to-noise ratio is enhanced by selecting second harmonics (2f), which solely originates from MLD, using a lock-in amplifier with reference to the magnetic rotation frequency. The portable equipment was able to detect ~40 parasites/μL (in ring stage) and even fewer, less than 10 parasites/μL (in later stages), with results available within 15 min. **b** Comparison of time intervals for drug susceptibility assay methods (RMOD, ELISA, DELI, and fluorescent SYBR Green dye) is depicted in blue, while the formation time of the corresponding targets (hemozoin, proteins, and DNA) is represented in black. Hemozoin-based RMOD technology is certainly capable of drug potency testing with much shorter incubation times (6–10 h) than standard assays (48–72 h). The figure is built upon the material adapted with permission from (**a**) ref. [74] Copyright 2020 Springer Nature (CC-BY-NC-SA 3.0) and ref. [159] Copyright 2021 Springer Nature (CC BY 4.0). (**b**) ref. [145] Copyright 2021 Springer Nature (CC BY 4.0).

β-hematin crystals in blood, down to a concentration of 0.015 μg/mL, which is mainly limited by a frequency-independent background signal, possibly originating from the Voigt effect of the medium. With this optimized setting, RMOD for in vitro cultured *P. falciparum* parasites achieved a detection capability down to ~40 parasites/μL of (lysed) blood in the ring stage and even less than 10 parasites/μL in the later stages of intra-

erythrocytic malaria cycle.[142] The RMOD methodology is further validated in mice studies,[143,144] revealing highly sensitive (not less than light microscopy) in vivo monitoring of hemozoin production during progression and clearance dynamics during and after the treatment. The RMOD technology also demonstrated a quantitative assessment of antimalarial drug potency[145] at very short incubation times of 6–10 h compared to conventional methods [see Fig. 9b]. The authors intend to examine RMOD capability for the assessment of drug inhibitory effects in a stage-specific format.

The magnetism of hemozoin was recently employed in a magneto-chromatography online device,[146,147] wherein i-RBCs were magnetophoretically concentrated (in a gradient magnetic field by SPM microbeads), and hemozoin crystals were isolated by rinsing in an alkaline solution and quantified by optical spectrophotometry. This methodology can detect hemozoin concentrations down to 0.033 μg/mL of whole blood, broadly equivalent to 55 parasites/μL in in vitro cultured samples, within 15 min.

Another methodology to measure tiny magnetic signals is magnetic resonance-based techniques using optically active spin defects, such as NV centers in diamond.[82–84] NV-based diamond quantum sensors have shown a sensitivity down to a single nuclear (electron) spin at room temperature, compared to the minimum 10^{12} (10^{9}) nuclear (electron) spins typically needed for conventional MRI. NV-ODMR technology, with the striking blending of high sensitivity and nanoscale resolution, has previously shown excellent promise for biosensing,[148] including single DNA,[149,150] living cells,[151] magnetically labeled cancer cells,[152] single proteins[153] and neurons,[154] among others. Fescenko et al.[87] have recently demonstrated its potential for detecting individual hemozoin nanocrystals, with the promise of a highly sensitive, label-free malaria diagnostic.

Field evaluation

After the successful demonstration of hemozoin sensing-based diagnostics in in vitro studies involving cultured *P. falciparum* parasites or *β*-hematin in blood suspensions in a laboratory setting, various of these methodologies have been evaluated for sensitivity (true positive rate) and specificity (true negative rate) in field/clinical setting. The magnetic-based NMR relaxometry technique was evaluated in an animal (mice) study[58] in a blinded test on a large sample scale ($n = 58$). For the early stage of infection (for initial 6 days), micro-NMR demonstrated high sensitivity and specificity of 97.9% and 90%, respectively, outperforming blood-smear microscopy, which had a sensitivity of 774.9% and specificity of 82%. Furthermore, the non-invasive diagnostic functionality of different hemozoin sensing technologies has also been exploited in animal studies.[106,115]

TMek technology, developed by Bertacco and co-workers[79,102] in 2020, was applied in a preclinical study in Cameroon, using light-microscopy as a reference measurement. TMek was evaluated with blood samples ($n = 75$) from peripheral (venous), while only a few ($n = 10$) samples were taken using a capillary (finger prick). The two methodologies gave no false negative results, proving a 100% sensitivity of TMek. The test with capillary samples also gave no false negatives, resulting in a specificity of 100%. On the contrary, large-scale testing with peripheral samples gave 9 false positives, leading to a specificity of 69%. This discrepancy may arise from the fact that fingerprick samples were tested within 5 hours, while peripheral samples were examined up to 16 h after sampling. Furthermore, hemoglobin (in healthy samples) can degrade to met-Hb, resulting in paramagnetic corpuscles (with magnetic susceptibility close to i-RBCs), leading to false positives. Nevertheless, TMek with prick-test, despite testing on a small sample scale, promises a highly sensitive and specific malaria diagnosis in a clinical setting.

The ATR-FTIR technology, developed by Wood and his team,[134] was first evaluated in a field trial in a malaria-endemic country, namely Thailand.[155] The blood samples from 318 patients were acquired in four regional clinics and tested using two portable ATR–FTIR spectrometers operated via a user-friendly software interface to the "Cloud". An independent test set based on PCR assay results was used as the "gold standard" to cross-validate the spectroscopic analysis. Data were analyzed using a machine learning classification (support vector machines; SVM), which yielded a 92% sensitivity and 97% specificity. This outperformed PLS-DA modeling, which achieved 90% sensitivity and 91% specificity. Similarly, Mwanga et al.[156] demonstrated the potential of ATR–FTIR spectroscopy coupled with supervised machine learning to diagnose malaria in human dried blood spots (DBS) obtained from field surveys of naturally infected individuals in a malaria-endemic community in Tanzania. The study considered 296 samples in total and supervised logistic regression models attained sensitivity and specificity of 91.7% and 92.8%, respectively for predicting *P. falciparum* infections, whereas 85% and 85%, respectively for predicting mixed (*P. falciparum* and *P. ovale*) infections.

The magneto-optical diagnostics (MOD) tool, developed by Newman and co-workers,[138] was tested on 217 clinical samples comprising patients with malaria and other diseases (e.g., sickle cell anemia) from endemic countries and healthy non-endemic controls. In a pre-examination, light microscopy confirmed that samples could be quantified to a parasitemia level ≥600 parasites/μL. The MOD technique diagnosed the (lysed) blood samples with a sensitivity and specificity of 78.8% and

74.6%, respectively, when using the PCR assay as the reference standard. The false positive rate was contributed by sickle cell patients and, more worryingly, from healthy controls, which was attributed to contaminations from the assembly process and/or blood lysing. Notably, MOD was performed on long-stored blood samples, which may have resulted in hemozoin agglutination (with no magneto-optical response), contributing to false negatives. The false signals may also be originated by differences in hematocrit levels for individuals. The team also examined another magneto-optical technology, accounting for MLD of hemozoin, on a small scale of 13 patients (including sickle cell anemia) and successfully diagnosed in agreement with RDTs.[137] The MLD-based non-invasive magneto-optic (NIMO) device is also evaluated in a fingertip probe on a small sample of 46 patients using light microscopy as the reference technique.[141] This gave a low sensitivity of 26.7% and a moderate specificity of 80.6%. Yet, as a non-invasive diagnostic, it is highly encouraging. The authors addressed this low sensitivity as a consequence of the man-machine interface (constant finger position and pressure).

Another portable MOD device, Gazelle (LoD = 50 parasites/μL),[139] were tested on (lysed) blood samples from 262 febrile patients with microscopy-confirmed (*P. falciparum* and *P. vivax* infected) samples having parasitemia ≥ 41 parasites/μL. The device diagnosed the samples within 1 min with an overall sensitivity and specificity of 97.6% and 96.8% (with 100% accuracy for *P. vivax* infections only) using light microscopy as the reference standard. However, the overall sensitivity decreased noticeably to 82.1%, using the PCR assay as the reference standard. The sensitivity improved to 85.4% upon exclusion of patients with a recent malaria history. Following this development, Gazelle conducted a study on 276 and 180 specimens (with *P. vivax* infections only) from the Brazilian[157] and Peruvian Amazon,[158] respectively, revealing a sensitivity of 72.1% and 88.2% using PCR as the gold standard. More specifically, the sensitivity for specimens with parasitemia>200 parasites/μL achieved 98.67%, however, it decreased to 12.5% for lower parasitemia.[158]

MLD-based RMOD technology[74] was also examined on clinical samples from 956 suspected malaria patients in a high-transmission region.[159] Samples from malaria-naive volunteers were considered as a background for the MLD signal, however, most malaria-negative samples (from light microscopy as gold standard) showed a higher signal than the background. Therefore, a considerably higher cut-off level (for decision-making) was set to achieve the best overall sensitivity and specificity of 82% and 84%, respectively. This improved to 87% and 88%, respectively for only *P. vivax* infections (due to a 10-fold higher average magneto-optical signal). The overall sensitivity also improved to 86% upon exclusion of samples from recently infected patients in high-transmission settings. The authors hypothesized the persistence of a significant amount of hemozoin in peripheral blood in a considerable population in high-transmission settings. More importantly, the determination of a cut-off MLD level relies on using a conventional diagnostic method. Nevertheless, in low-transmission settings, the cut-off level, particularly for *P. vivax* infections, should approach the background signal (from naive samples), leading to a significantly improved malaria diagnosis.

Outlook

Critical for the control and elimination of malaria is a rapid and accurate (quantitative) diagnosis of the disease, including the capacity to have ultra-sensitive and highly specific detection (Plasmodium species identification) in early (ring and early trophozoite) stages, and to identify the appropriate anti-malarial drug for the treatment. None of the current clinical methods (e.g., light microscopy, molecular approaches, and serological tests) offer these functionalities in a single test [see Table 3 and Fig. 10]. With this respect, the emergence of hemozoin-based point-of-care technologies augurs well to achieve the required sensitivity in a rapid time to stratify asymptomatic individuals in malaria high-transmission regions. The rich magnetic and optical properties of hemozoin due to the presence of unfilled electrons in the sub-orbitals of Fe^{3+} ions make hemozoin an excellent target not only for clinical diagnosis but also provide unique information for designing and clinical testing novel anti-malarial drugs at very short incubation times in comparison to conventional techniques [see Table 4].

In the search of appropriate anti-malarial drug resistance, the essential question is how malaria parasites cope with toxic (free) heme, or, more specifically, how hydrogen bonding in the hemozoin crystal occurs and whether this is a nonenzymatic or enzymatic process.

The recent application of high-resolution microscopy methods such as electron microscopy, soft X-ray tomography, etc.[46,51,160] has offered a better understanding of crystal morphology, growth medium, and important factors leading to crystal growth and inhibition. However, the origin of hemozoin nucleation is still unresolved. The reason is understanding hydrogen-bonding networks in such nanocrystals with traditional X-ray crystallography methods is difficult. Using advanced 3D electron diffraction,[161] Matz et al. demonstrated that the technique was capable of determining the hemozoin crystalline order under the deregulation of PbPV5 proteins in vivo.[51] Meanwhile, electron diffraction also often suffers from accuracy issues related to H-atom positions and identifying atoms with similar atomic numbers (carbon, nitrogen, and oxygen). In such a case, the combination of

Table 3 The comparison of malaria diagnostic techniques based on bioinert malaria pigment, hemozoin, and other biomolecule-based techniques.

Omics	Target	Diagnostic property	Technology platform	Species/ material	Sensitivity (%)	Specificit (%)	LoD (p/uL)	Time (min)	Study	Reference
Molecular	rRNA		PCR variants	P(f,v,o,m)	>98	>88	<2 Pf	> 120	Field setting	[10]
			LAMP	P(f,v)	>98.3	>94.3	<5	< 60	Field setting	[10]
Serological	HRPII		RDT	P(f,v,o,m)	>85	>95.2	<100	< 20	Field setting	[10]
Microscopy	i-RBCs		Lignt microscopy	P(f,v,o,m)	95	98	>50[a]	60	Field setting	[10]
Inorganic Crystal	Hemozoin	Magnetic	micro-NMR	Pf, Pb	97.9	90	<10 (R)	5	Animal Study	[58]
			TMR chip	–	–	–	150 pT	–	Proof-testing	[101]
			TMek chip	P(f,v,o,m)	100	69/100[b]	10	<20	Field setting	[79]
		Optical	Absorbance	Py	–	-	<0.03%	<1	Animal Study	[106]
			Absorbance	β-hematin	100	96.3	1 μg/mL	6	Proof-testing	[103]
			Reflectance	Pf	–	–	12	–	Proof-testing	[107]
			PA-SAW	Pf	–	–	1% (R)	<2	Proof-testing	[111]
			H-VNB	P(f,v)	–	–	5/17[c]	<1	Animal Study	[115]
			THG Imaging	Pf	–	–	<0.2%[d]	<15	Proof-testing	[116]
			ATR-FTIR	P(f,v)	92	97	0.5 Pf (R)	<5	Field setting	[155]
		Optical-SERS	SERS: Magnetic	β-hematin	–	–	5 nM	>49	Proof-testing	[123]
			SERS: butterfly	Pf	-	–	25 (R)	<15	Proof-testing	[125]
			SERS: AgNPs	Pf	–	–	2.5 (R)	>43	Proof-testing	[126]
			SERS: AuNS	P(f,v)	100	100	0.1 Pf	30	Field setting	[129]
			SERS on chip	Pf	–	–	125 (R)	>10	Proof-testing	[128]
		Magneto-Optical	MOD	P(f,v,o,m)	78.8[e]	74.6[e]	5 ng/uL	1	Field setting	[138]
			Gazelle	P(f,v)	98 (82.1[e])	97 (99[e])	50 Pf	<1	Field setting	[139]
			Portable MOD	β-hematin	–	–	8.1 ng/mL	10	Proof-testing	[140]
			NI-MOD	Pf	26.7	80.6	<1 μg/mL	<1	Field setting	[141]
			RMOD	P(f,v)	82(78)[e]	84 (78)[e]	40 Pf (R)	<15	Field setting	[159]
			Magneto-chromatography	Pf	–	–	55	<15	Proof-testing	[147]
			NV-ODMR	Pf	–	–	≃1.4 μT[f]	–	Proof-testing	[87]

[a]The LoD depends on microscopist experience. An expert microscopist may reach to a limit of 4–20 parasites/μL.
[b]TMek was examined in two methods, first with peripheral (venous) and second with capillary (finger prick) samples.
[c]H-VNB approach was examined in both in vitro (human blood) and in vivo (transdermal detection in animals) methods.
[d]THG imaging was validated for parasitemia as low as 0.2% in blood from malaria patients. In principle, less than 5 parasites per field of view were detected.
[e]The sensitivity and specificity are compared to the PCR method as a reference standard.
[f]NV-ODMR could demonstrate magnetic mapping of individual "solitary" hemozoin crystals, but LoD in parasites/μL is not defined.
The sensitivity and specificity are compared to microscopy, whereas the microscopy method is compared to polymerase chain reaction (PCR). In the limit of detection (LoD) column, the (R) represents the detection limit in the early "ring" stage of the malaria erythrocyte cycle. For comparison, 0.0001% parasitemia ≈5 parasites/μL ≈ 0.003 μg/mL (in the mature stage, 50% hemoglobin to hemozoin conversion).[137]

electron and NMR crystallography has been shown to be effective in elucidating complex hydrogen-bonding structures.[162] Future research seeks such advanced investigation of the heme detoxification process in vivo to better understand the mechanisms underlying hemozoin nucleation for the development of effective antimalarial drugs.

The peculiar magnetism in hemozoin has received progressively increasing attention, both for understanding at the fundamental level and its use as a tool for malaria diagnostics. The magnetometry studies, mostly via lab-grown β-hematin[74,76–78] suggest a puzzling PM/SPM ground state, although primary NV-ODMR experiments[87] put forward a SPM-like behavior for very small crystals, whereas a PM behavior for bigger crystals. This contradicts the expected SPM-FM transition, as the crystal size increases, in conventional nanomagnets.[80,81] Moreover, natural hemozoin typically has a long axis of 200–600 nm, primarily depending upon the Plasmodium species.[37] Thus, future magnetic studies on hemozoin/β-hematin with controlled variation in crystal size and shape will help to better understand its magnetic ground state and exploit it for stage- and species-specific diagnostic. Despite a lack of clarity in the magnetic picture of hemozoin, it is employed in various magnetic-based malaria diagnostic techniques. Meanwhile, it is observed that ingestion of hemoglobin by Plasmodium parasites initiates two simultaneous processes: free heme is converted to hemozoin crystals,[30] as well as hemoglobin is oxidized into metHb,[27] both containing Fe^{3+} (high-spin $S = 5/2$, paramagnetic) ions. Furthermore, ingestion of metHb releases non-heme iron undergoing accumulation into ferritin or hemosiderin,[163] which are also SPM in nature.[164] Thus, malaria-infected i-RBCs also have a magnetic background signal from (specific to individual) non-hemozoin magnetic entities[55] i.e., iron-rich hemoglobin in different forms,

which recommends advanced data analysis methods like machine learning to speed up the field-implementation of magnetic technologies.

Very recently, Kung et al. exploited machine learning to understand the complex, yet specific and unique molecular fingerprinting of a single drop of blood.[61,165] The group developed a new methodology to capture the 2D T_1–T_2 (NMR) correlational spectroscopy by harvesting the highly efficient multidimensional inverse Laplace decomposition technique. Machine learning techniques were introduced to reduce the dimensionality by transforming the complex 3D contour plots (from 2D NMR measurements) into 2D scatter plots and user-friendly information for point-of-care disease diagnosis and monitoring [see Fig. 11]. The clinical application of this technology enables the direct analysis of human whole blood in various physiological (e.g., oxygenated/deoxygenated states) and pathological (e.g., blood oxidation, hemoglobinopathies) conditions.[24,93] A highly time- and patient-specific 'molecular fingerprint' can be obtained in minutes. In a blind test on 32 anonymized subjects, the supervised learning models demonstrated a higher sensitivity of 88.5% and specificity of 88.7% within 30 s, outperforming trained technicians with 81.1% sensitivity and 72% specificity in 10 min. Thus, the higher order of (pseudo-)dimensionality (e.g., 2D- or multi-dimensional) in time-domain NMR coupled with machine learning may substantially improve the speed and accuracy of object identification.[61,100] This technique can be directly applicable to malaria infection[17,99] and such progress is currently under way.

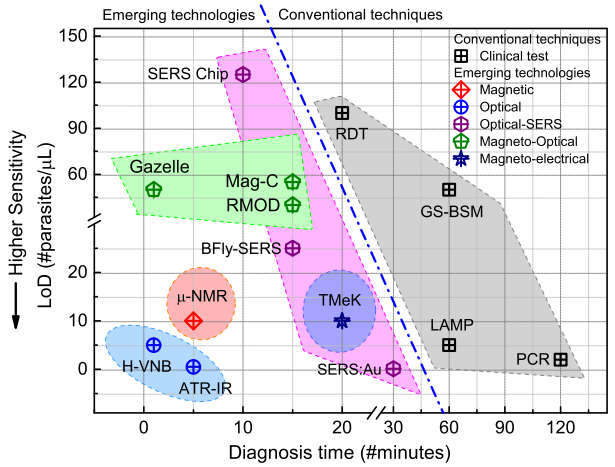

Fig. 10 Mapping of malaria diagnostic technologies with respect to sensitivity and diagnosis time. A comparative analysis of conventional clinical methods against state-of-the-art (magnetic, optical, magneto-optical & electrical) technologies targeting hemozoin as a biomarker. The characteristics numbers for each technology are taken from Table 3, wherein the original articles are cited. GS-BSM Giemsa-stained blood-smear microscopy, PCR polymerase phain reaction, LAMP Loop-mediated isothermal amplification, RDT rapid diagnostic test, SERS Surface enhanced Raman spectroscopy, BFly-SERS SERS with butterfly wings, NMR Nuclear Magnetic Resonance, H-VNB hemozoin-induced vapor nanobubbles, ATR-IR Attenuated Total Reflectance - infrared spectroscopy, RMOD Rotating-crystal magneto-optical diagnostic, and Mag-C Magneto-chromatography.

Exploiting nanofabrication has revolutionized medical diagnostic methods as new detection modalities and transducers were invented. Magnetic nanotechnologies, such as TMR,[101] have shown considerable potential in detecting malaria. The ability to integrate spintronic sensors based on the TMR effect into standard complementary metal-oxide semiconductor (CMOS) wafers is a fundamental step toward large-scale production,

Table 4 The comparison of antimalarial drug testing methods based on bioinert malaria pigment, hemozoin, and other biomolecule-based techniques.

Target	Property	Technology platform	Anti-malarial drug/s	Incubation time (h)	Reference
DNA		PCR/MSF	AM, AS, CQ, MFQ, QN, PPQ	48	194
HRPII		RDT/ELISA	AM, AS, CQ, MFQ, QN, PPQ	48-72	195
i-RBCs		Light microscopy	AM, CQ, MFQ, QN, PRM, ADQ	24-30	196
Hemozoin	Magnetic	NMR relaxometry	AM & CQ	6-24	98
	Optical	Raman	CQ	20	197
		TERS	CQ	17	198
		ATR-FTIR & Raman	CQ	5	199
		UV-visible-NIR	AM & MFQ	10-11	200
		Flow-Cytometry	AM, AS, CQ, MFQ, QN, PRM	18-24	201
	Magneto-Optical	RMOD	AM, PPQ & CQ	6-10	145

Abbreviations: *MSF* malaria SYBR green I fluorescence, *ELISA* enzyme-linked immunosorbent assay, *TERS* tip-enhanced Raman scattering, *AM* artemisinin, *AS* artesunate, *CQ* chloroquine, *MFQ* mefloquine, *QN* quinine, *PPQ* piperaquine, *PRM* pyrimethamine, *ADQ* amodiaquine.

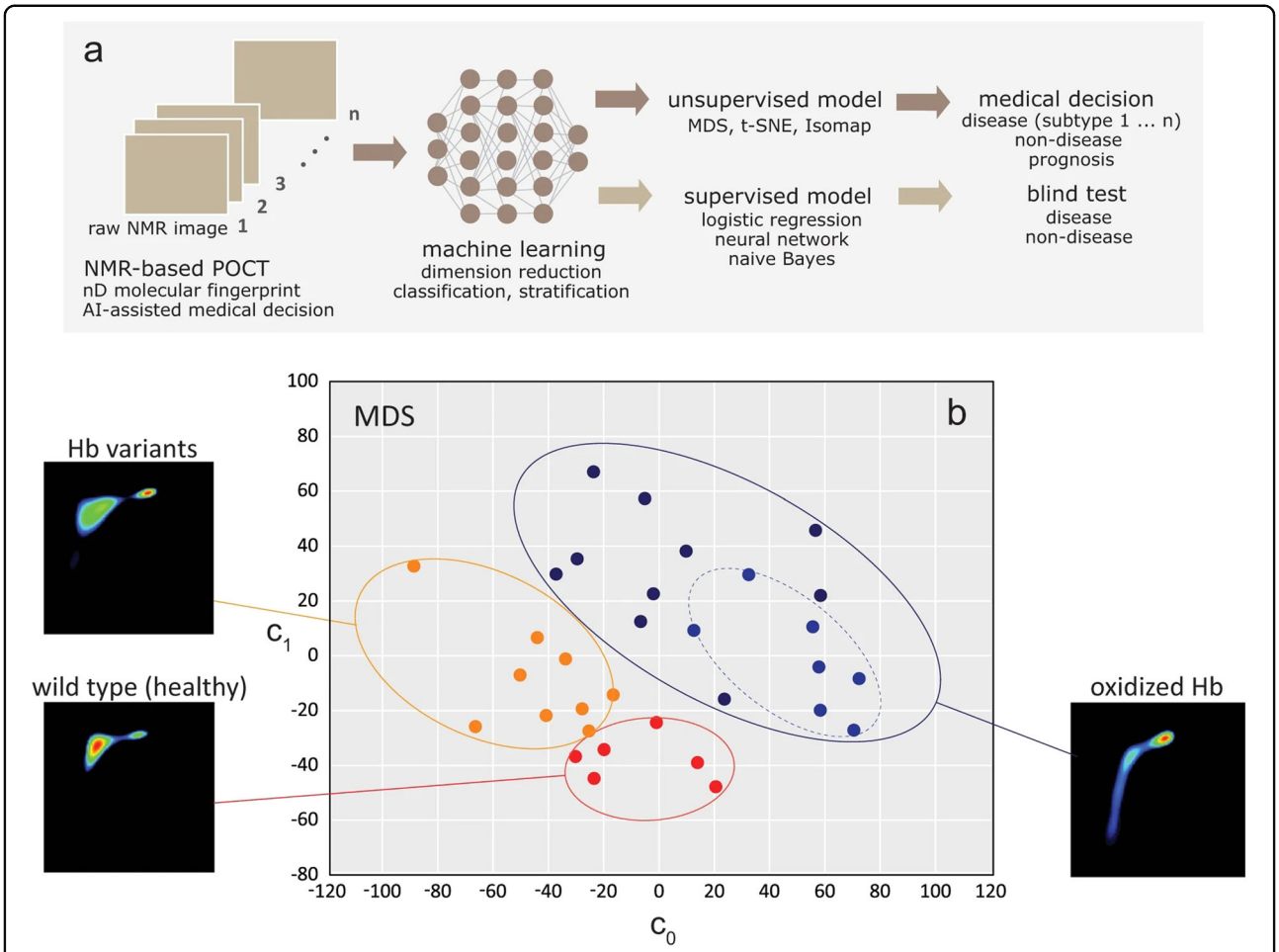

Fig. 11 Machine-learning assisted NMR-based point-of-care technology (PoCT) in making medical decisions. a the workflow of machine learning in processing the complicated raw data into user-friendly medical decisions (e.g., disease subtyping). The raw T_1–T_2 correlational data are firstly converted into machine language by pre-trained image embedding (e.g., SqueezeNet) features, which are fed to unsupervised/supervised learning models. Unsupervised techniques are used to reduce data dimensionality and convert it into human-friendly 2D-scatter plots (e.g., multidimensional scaling (MDS)) and classification (e.g., hierarchical clustering) into **b** disease (oxidized Hb), non-disease (healthy wild type) and mutated counterpart (Hb variants) clusters. Furthermore, disease subtypes (sub-type 1: oxidized Hb, sub-type 2: partially oxidized Hb) are also identified. The clustering circles are drawn for eye-balling purposes. On the other hand, supervised learning models (e.g., neural network, logistic regression, and naïve Bayes) are used for a blind test to evaluate the machine performance against human beings. The figure is adapted with permission from ref. [61] Copyright 2020 Springer Nature (CC BY 4.0).

dissemination, and commercialization of the research. Furthermore, the integration of spintronics and CMOS technology can create hybrid devices with functionalities that are not available in either of the two individual technologies. Further improvement of the TMR-based diagnostic device will open new possibilities for the early-stage detection of malaria. The microchip-based TMek[79] is a quantitative and stage-selective diagnostic tool for an effective screening of the population but improvements in apparatus engineering, scaling up chip production, and advanced decision-making are needed to mature the technology for field deployment.

The optical properties of hemozoin have been harnessed in numerous technologies, as discussed in "Optical-based technology", to enable a rapid and sensitive malaria diagnosis at a low cost. In pursuit of this goal, reflectance spectrophotometry[107] has demonstrated its potential for early and sensitive malaria diagnostics using thin film (band-pass) filters. These characteristics can be further improved through optimized fabrication, better materials, and the inclusion of additional commercial filters. It is suggested that an accurate algorithm may further enhance decision-making for a more specific diagnostic. The authors aim to integrate these filters into a single chip for non-invasive malaria diagnosis among asymptomatic individuals in high-transmission settings.

Another optical-based fingerprint of malaria is Raman spectroscopy of hemozoin. However, in its spontaneous

form, sensitivity is too low for early diagnosis, even with resonant excitation and magnetic field enrichment[123] and optical tweezers.[166] Subsequent studies have explored various metallic nanostructures to enhance the Raman cross-section of hemozoin, resulting in ultrasensitive malaria diagnosis.[126,129] Nonetheless, the instantaneous growth of nanostructures requires a laboratory setting and is time-consuming, while their short shelf-life on a commercial scale poses a challenge. Other approaches have attempted to use naturally occurring nano-structures[125] and on-chip nanostructures growth,[128] but a propensity for hemozoin aggregation and the conversion of healthy hemoglobin to hematin in these approaches may limit their clinical performance. In a close development, antigen-based SERS testing on 190 clinical samples from endemic regions[167] differentiated between Ebola and malaria with high specificity of 97.9% and 99.6%, respectively. However, this method is also time-consuming (30 min). Overall, the rapid, consistent, and uniform synthesis of SERS agents, especially on micro-optofluidic chips,[168] remains an open question for achieving rapid and accurate malaria diagnosis.

In optical technologies, spectroscopy-based ATR–FTIR sensing of hemozoin, with the aid of machine learning, has demonstrated its highest potential for point-of-care malaria diagnosis in two clinical studies conducted in low-resource settings within malaria-endemic countries.[155,156] ATR–FTIR is both cheap and easy to use, requiring minimal expertise and little to no sample preparation. However, improvements are required to expedite the measurements, including the drying procedure and subsequent cleaning of the ATR crystal. To address this concern, an affordable, disposable coverslip[169] has been proposed to facilitate the collective drying of multiple samples for successive measurements. PLS-RA has exhibited the ability to detect and quantify parasitemia in the 0–5% range. More recently, NIR spectroscopy has been applied to malaria diagnosis. Notable research in this regard is the successful detection and quantification of P. falciparum-infected malaria in dried blood samples using a "Matchbox" size spectrometer[170] and aqueous blood samples using a combination of NIR and UV-visible spectroscopy.[171] In a recent study, visible micro-spectrophotometry was applied to discriminate the different stages of asexual blood stages of *P. falciparum* parasites at single cell level in functional erythrocytes.[172]

The success of machine learning with 2D NMR relaxometry and ATR–FTIR techniques inspires us to exploit it for extracting maximum information from hemozoin-based malaria diagnostics. Deep learning and machine learning methods have recently accomplished a significant breakthrough in automating the conventional microscopic examination of malaria in the perspective of sensitivity and reduced labor-force. An exceptional accuracy of up to 99.9% has been achieved.[173–177] However, reliability still poses a significant challenge as humans are widely regarded to have superior judgment as compared to computer algorithms. Nonetheless, deep learning models have reportedly made significant advancements in recent times, indicating the potential for machines to eventually take over human tasks. Indeed, there is a surge in the utilization of machine learning for novel medical diagnostics.[178,179] Of relevance to us, its combination with Raman spectroscopy has offered a high sensitivity to any tiny changes in spectral features for different biological entities,[180] resulting in significant improvements in diagnostic capabilities for a number of diseases e.g., hepatitis B,[181] typhoid and dengue infections,[182] etc. Of great interest, this combination can classify the malaria-infected and dengue-infected donors with an efficiency of 83.3%, while individually achieving a diagnostic sensitivity/specificity of 95.29% and 95.84%, respectively, against healthy control groups, respectively.[183] More recently, Raman spectroscopy using PCA-DA successfully diagnosed COVID-19 infection with 87% sensitivity and 100% specificity.[184] In a preliminary study,[185] ATR–FTIR spectroscopy was also exploited for the rapid diagnosis of COVID-19, with machine learning analysis predicting it with a moderate accuracy of 78.4%. Wood and co-workers[186] explored transflection infrared spectroscopy to diagnose COVID-19 in saliva samples. Transfection offers several advantages over ATR–FTIR, including batch sample drying, infrequent instrument cleaning (to avoid health risks for healthcare workers), and approximately three times larger light absorbance. Overall, spectroscopy-based Raman, ATR–FTIR, and NIR (or a combination of them) with machine learning analysis can help to stratify malaria from other similar symptomatic diseases, such as dengue and COVID-19, from a single sample, particularly in the current pandemic scenario.[7]

Magneto-optical technologies, primarily developed in a portable format, offer a rapid diagnostic approach for field conditions, proving especially effective in low-resource settings. In both the methodology, simplest MOD (e.g., Gazelle) and MLD (e.g., RMOD) devices demonstrated a satisfactory performance, particularly for *P. vivax* infections (a major portion of infections outside endemic areas), with sensitivities on par with or superior to light microscopy. However, these studies have identified several key factors responsible for degradation in their performance. The primary challenges are the need for fresh samples (to avoid hemozoin agglutination) and blood lysing. Similar kinds of other diseases (e.g., sickle cell anemia) affecting magnetic fingerprints of blood and the potential persistence of residual hemozoin from previous infections in endemic regions can contribute to false signals. Additionally, variable hematocrit levels among

individuals and associated background signals introduce further complexity to the decision-making process. These challenges highlight the necessity for several levels of advancements, such as the integration of microfluidics and algorithmic decision-making with machine learning, to enhance diagnostic performance.

Another magneto-optic-based NV-ODMR technology has demonstrated the capability to image the individual hemozoin nanocrystals.[87] In the bio-physical processes, the capability of detecting the molecular machinery remains a significant technological challenge, primarily due to poor sensitivity and/or selectivity and specific sample requirements for most bioimaging methods. In recent years, NV sensors have been successfully employed for imaging various biomedical samples, including single living cells, under ambient conditions.[148] These NV-based ultrasensitive experiments, however, incorporate several bulky and expensive components in a laboratory-based setting, typically utilizing table-top confocal optical systems for single NV measurements. Consequently, the large size and complexity of these setups make them unsuitable for diagnostic applications in field conditions. Nevertheless, work is rapidly progressing on the miniaturization of NV-based diamond quantum sensors, featuring simpler optical setups, into a simplified and transportable form.[187–190] This can offer one of the best tools for bioimaging and biodiagnostics available today. NV-based measurements can also play a part in understanding the developmental stages of malaria, particularly by monitoring the formation of single hemozoin nanocrystals in living Plasmodium-infected cells, shedding new light on the hemozoin nucleation mechanism and the discovery of novel antimalarial drugs.

Concluding remarks

Currently, many hemozoin-based diagnostic technologies are able to compete with, or even outperform, conventional microscopy and RDT methods, offering notably higher sensitivity (approaching PCR-based methods) and delivering rapid results within a few minutes.

The primary challenges before hemozoin-based diagnostic to reach an ideal format are species-specific diagnosis and the ability to distinguish fresh hemozoin, generated within i-RBCs, from the residual content within white blood cells (WBCs) resulting from phagocytosis of hemozoin in previous malaria infections. Several hemozoin-based research groups[99,139,159] are currently aspiring for future improvements in species differentiation by leveraging hemozoin crystal morphology (size and shape),[37] and exploring multi-dimensionality in time-domain NMR with the aid of machine learning,[59,61] etc. On another front, an in vivo optical absorbance study, involving mice, has demonstrated the potential to discriminate hemozoin in i-RBCs and WBCs based on intensity features and hemozoin crystal size, and the results were validated with similar findings for *P. falciparum* blood smears with conventional light microscopy.[191] Nevertheless, it is worth noting that hemozoin gets cleared from the bloodstream within a few days,[37] in contrast to the longer persistence of antigens (e.g., HRPII and LDH), which can remain detectable for several weeks to more than a month.[192] These factors recommend hemozoin sensing over RDT for a more accurate diagnosis.

In summary, ultrasensitive hemozoin-based techniques are being developed with tremendous potential for early and highly specific malaria diagnosis. These methods can also contribute to the development of targeted drugs and vaccines to combat the disease. Nevertheless, several technical challenges must be addressed to achieve their highest potential, especially as scalable and cost-effective technologies suitable for field deployment in remote, under-resourced regions where malaria is endemic. As research is rapidly progressing toward the development of inexpensive, miniaturized, or lab-on-chip devices that can be battery-powered, the tantalizing prospect of personalized medicine is on the horizon. Integrating mobile phones with diagnostic tools enables data to be sent to the Cloud and analyzed in real-time.[155] The mobile interface also provides a global positioning system that can be used for epidemiological surveillance.

Machine learning, which makes machines smarter, has become more popular of late, and it is likely another game-changer that can expedite the field implementation of emerging spectroscopic-based technologies for malaria eradication and elimination strategies in the future. Human being is slowly (but surely) in winning the race over the war of malaria. Strong political will (e.g., human capital, funding agency), however, is needed to accelerate the translation of these technologies into field settings, as most of these endemic regions are in developing regions.

Acknowledgements

W.K.P. acknowledges the Frontier Research Grant of Songshan Lake Materials Laboratory and NSFC International Excellent Young Scientists (T2350610282). V.P.B. acknowledges the financial support from DST QUEST grant DST/ICPS/QuST/Theme-2/Q35 and the Institute of Eminence scheme at IIT-Madras, through the Quantum Center of Excellence for Diamond and Emergent Materials (QuCenDiEM) group. H.H. acknowledges the EPSRC Impact Acceleration Account (IAA) under grant EP/R511705/1, MAGNOSTIC: Novel non-Invasive Magnetic-based Malaria Diagnostic Sensor.

Author details

[1]Quantum Center of Excellence for Diamond and Emergent Materials, Indian Institute of Technology Madras, Chennai 600036, India. [2]Department of Physics, Indian Institute of Technology Madras, Chennai 600036, India. [3]Department of Electrical Engineering, Indian Institute of Technology Madras, Chennai 600036, India. [4]Microelectronics Lab, James Watt School of Engineering, University of Glasgow, Glasgow G12 8QQ, UK. [5]Centre for Biospectroscopy and School of Chemistry, Monash University, Clayton, Vic 3800, Australia. [6]Songshan Lake Materials Laboratory, Building A1, University Innovation Park, Dongguan 523808, China

Author contributions
W.K.P. and A.R. initiated the idea and prepared the first draft. All authors wrote and commented on the paper.

Competing interests
The authors declare no competing interests.

Publisher's note
Springer Nature remains neutral with regard to jurisdictional claims in published maps and institutional affiliations.

Received: 14 February 2023 Revised: 20 October 2023 Accepted: 27 October 2023.
Published online: 22 December 2023

References

1. Organization, W. H. et al. World malaria report 2020: 20 years of global progress and challenges (2020).
2. Organization, W. H. Global technical strategy for malaria 2016–2030 (2015).
3. Menard, D. & Dondorp, A. Antimalarial drug resistance: a threat to malaria elimination. *Cold Spring Harb. Perspect. Med.* **7**, 025619 (2017).
4. Organization, W. H. et al. *World Malaria Report 2021* (2021).
5. Rts, S.: Clinical trials partnership. Efficacy and safety of RTS, S/AS01 malaria vaccine with or without a booster dose in infants and children in Africa: final results of a phase 3, individually randomised, controlled trial. *Lancet* **386**, 31–45 (2015).
6. Calderaro, A. et al. Malaria diagnosis in non-endemic settings: the European experience in the last 22 years. *Microorganisms* **9**, 2265 (2021).
7. Nghochuzie, N. N., Olwal, C. O., Udoakang, A. J., Amenga-Etego, L. N.-K. & Amambua-Ngwa, A. Pausing the fight against malaria to combat the covid-19 pandemic in Africa: is the future of malaria bleak? *Front. Microbiol.* **11**, 1476 (2020).
8. Aborode, A. T. et al. Fighting covid-19 at the expense of malaria in africa: the consequences and policy options. *Am. J. Trop. Med. Hyg.* **104**, 26 (2021).
9. Organization, W. H. et al. *A Framework for Malaria Elimination* (2017).
10. Mbanefo, A. & Kumar, N. Evaluation of malaria diagnostic methods as a key for successful control and elimination programs. *Trop. Med. Infect. Dis.* **5**, 102 (2020).
11. Pham, N. M., Karlen, W., Beck, H.-P. & Delamarche, E. Malaria and the 'last'-parasite: how can technology help? *Malar. J.* **17**, 1–16 (2018).
12. Amir, A., Cheong, F.-W., De Silva, J. R. & Lau, Y.-L. Diagnostic tools in childhood malaria. *Parasites Vectors* **11**, 1–12 (2018).
13. Krampa, F. D., Aniweh, Y., Kanyong, P. & Awandare, G. A. Recent advances in the development of biosensors for malaria diagnosis. *Sensors* **20**, 799 (2020).
14. Coronado, L. M., Nadovich, C. T. & Spadafora, C. Malarial hemozoin: from target to tool. *Biochim. Biophys. Acta* **1840**, 2032–2041 (2014).
15. Baptista, V., Peng, W. K., Minas, G., Veiga, M. I. & Catarino, S. O. Review of microdevices for hemozoin-based malaria detection. *Biosensors* **12**, 110 (2022).
16. Baptista, V. et al. The future in sensing technologies for malaria surveillance: a review of hemozoin-based diagnosis. *ACS Sens.* **6**, 3898–3911 (2021).
17. Dupr´e, A., Lei, K.-M., Mak, P.-I., Martins, R. P. & Peng, W. K. Micro-and nano-fabrication nmr technologies for point-of-care medical applications—a review. *Microelectron. Eng.* **209**, 66–74 (2019).
18. Peng, W. K., Paesani, D. Omics meeting Onics: towards the next generation of spectroscopic-based technologies in personalized medicine. (Multi-disciplinary Digital Publishing Institute, 2019).
19. Cruz, A. & Peng, W. K. Perspective: cellular and molecular profiling technologies in personalized oncology. *J. Personalized Med.* **9**, 44 (2019).
20. Kasetsirikul, S., Buranapong, J., Srituravanich, W., Kaewthamasorn, M. & Pimpin, A. The development of malaria diagnostic techniques: a review of the approaches with focus on dielectrophoretic and magnetophoretic methods. *Malar. J.* **15**, 1–14 (2016).
21. Chen, K., Perlaki, C., Xiong, A., Preiser, P. & Liu, Q. Review of surface enhanced Raman spectroscopy for malaria diagnosis and a new approach for the detection of single parasites in the ring stage. *IEEE J. Sel. Top. Quantum Electron.* **22**, 179–187 (2016).
22. Perez-Guaita, D. et al. Parasites under the spotlight: applications of vibrational spectroscopy to malaria research. *Chem. Rev.* **118**, 5330–5358 (2018).
23. Goh, B. et al. The application of spectroscopy techniques for diagnosis of malaria parasites and arboviruses and surveillance of mosquito vectors: a systematic review and critical appraisal of evidence. *PLoS Neglect. Trop. Dis.* **15**, 0009218 (2021).
24. Loh, T. P., Peng, W. K., Chen, L. & Sethi, S. K. Application of smoothed continuous labile haemoglobin a1c reference intervals for identification of potentially spurious hba1c results. *J. Clin. Pathol.* **67**, 712–716 (2014).
25. Maier, A. G., Matuschewski, K., Zhang, M. & Rug, M. Plasmodium falciparum. *Trends Parasitol.* **35**, 481–482 (2019).
26. Miller, L. H., Ackerman, H. C., Su, X.-Z. & Wellems, T. E. Malaria biology and disease pathogenesis: insights for new treatments. *Nat. Med.* **19**, 156–167 (2013).
27. Francis, S. E., Sullivan, D. J. & Goldberg, D. E. Hemoglobin metabolism in the malaria parasite *Plasmodium falciparum*. *Annu. Rev. Microbiol.* **51**, 97–123 (1997).
28. Sigala, P. A. & Goldberg, D. E. The peculiarities and paradoxes of plasmodium heme metabolism. *Annu. Rev. Microbiol.* **68**, 259–278 (2014).
29. Kumar, S. & Bandyopadhyay, U. Free heme toxicity and its detoxification systems in human. *Toxicol. Lett.* **157**, 175–188 (2005).
30. Egan, T. J. Haemozoin formation. *Mol. Biochem. Parasitol.* **157**, 127–136 (2008).
31. Weissbuch, I. & Leiserowitz, L. Interplay between malaria, crystalline hemozoin formation, and antimalarial drug action and design. *Chem. Rev.* **108**, 4899–4914 (2008).
32. Herraiz, T., Guill´en, H., Gonz´alez-Pe˜na, D. & Ar´an, V. J. Antimalarial quinoline drugs inhibit β-hematin and increase free hemin catalyzing peroxidative reactions and inhibition of cysteine proteases. *Sci. Rep.* **9**, 1–16 (2019).
33. de Villiers, K. A. & Egan, T. J. Heme detoxification in the malaria parasite: a target for antimalarial drug development. *Acc. Chem. Res.* **54**, 2649–2659 (2021).
34. Slater, A. et al. An iron-carboxylate bond links the heme units of malaria pigment. *Proc. Natl Acad. Sci. USA* **88**, 325–329 (1991).
35. Slater, A. & Cerami, A. Inhibition by chloroquine of a novel haem polymerase enzyme activity in malaria trophozoites. *Nature* **355**, 167–169 (1992).
36. Pagola, S., Stephens, P. W., Bohle, D. S., Kosar, A. D. & Madsen, S. K. The structure of malaria pigment β-haematin. *Nature* **404**, 307–310 (2000).
37. Noland, G. S., Briones, N. & Sullivan, D. J. Jr The shape and size of hemozoin crystals distinguishes diverse plasmodium species. *Mol. Biochem. Parasitol.* **130**, 91–99 (2003).
38. Egan, T. J., Mavuso, W. W. & Ncokazi, K. K. The mechanism of β-hematin formation in acetate solution. parallels between hemozoin formation and biomineralization processes. *Biochemistry* **40**, 204–213 (2001).
39. Dorn, A., Stoffel, R., Matile, H., Bubendorf, A. & Ridley, R. G. Malarial haemozoin/β-haematin supports haem polymerization in the absence of protein. *Nature* **374**, 269–271 (1995).
40. Pisciotta, J. M. et al. The role of neutral lipid nanospheres in plasmodium falciparum haem crystallization. *Biochem. J.* **402**, 197–204 (2007).
41. Jackson, K. E. et al. Food vacuole-associated lipid bodies and heterogeneous lipid environments in the malaria parasite, *Plasmodium falciparum*. *Mol. Microbiol.* **54**, 109–122 (2004).
42. Egan, T. J. et al. Haemozoin (β-haematin) biomineralization occurs by self-assembly near the lipid/water interface. *FEBS Lett.* **580**, 5105–5110 (2006).
43. de Villiers, K. A. et al. Oriented nucleation of β-hematin crystals induced at various interfaces: relevance to hemozoin formation. *Cryst. Growth Des.* **9**, 626–632 (2009).
44. Hempelmann, E., Motta, C., Hughes, R., Ward, S. A. & Bray, P. G. *Plasmodium falciparum*: sacrificing membrane to grow crystals? *Trends Parasitol.* **19**, 23–26 (2003).
45. Kapishnikov, S. et al. Aligned hemozoin crystals in curved clusters in malarial red blood cells revealed by nanoprobe X-ray Fe fluorescence and diffraction. *Proc. Natl Acad. Sci. USA* **109**, 11184–11187 (2012).
46. Kapishnikov, S. et al. Oriented nucleation of hemozoin at the digestive vacuole membrane in *Plasmodium falciparum*. *Proc. Natl Acad. Sci. USA* **109**, 11188–11193 (2012).
47. Mullick, D. et al. Diffraction contrast in cryo-scanning transmission electron tomography reveals the boundary of hemozoin crystals in situ. *Faraday Discuss.* **240**, 127–141 (2022).
48. Jani, D. et al. Hdp—a novel heme detoxification protein from the malaria parasite. *PLoS Pathog.* **4**, 1000053 (2008).

49. Chugh, M. et al. Protein complex directs hemoglobin-to-hemozoin formation in *Plasmodium falciparum*. *Proc. Natl Acad. Sci. USA* **110**, 5392–5397 (2013).
50. Matz, J. M. & Matuschewski, K. An in silico down-scaling approach uncovers novel constituents of the plasmodium-containing vacuole. *Sci. Rep.* **8**, 1–12 (2018).
51. Matz, J. M. et al. A lipocalin mediates unidirectional heme biomineralization in malaria parasites. *Proc. Natl Acad. Sci.* **117**, 16546–16556 (2020).
52. Pauling, L. & Coryell, C. D. The magnetic properties and structure of hemoglobin, oxyhemoglobin and carbonmonoxyhemoglobin. *Proc. Natl Acad. Sci. USA* **22**, 210–216 (1936).
53. Coryell, C. D., Stitt, F. & Pauling, L. The magnetic properties and structure of ferrihemoglobin (methemoglobin) and some of its compounds. *J. Am. Chem. Soc.* **59**, 633–642 (1937).
54. Weiss, J. J. Nature of the iron–oxygen bond in oxyhaemoglobin. *Nature* **202**, 83–84 (1964).
55. Hackett, S., Hamzah, J., Davis, T. M. & St Pierre, T. Magnetic susceptibility of iron in malaria-infected red blood cells. *Biochim. Biophys. Acta* **1792**, 93–99 (2009).
56. Furlani, E. Magnetophoretic separation of blood cells at the microscale. *J. Phys. D* **40**, 1313 (2007).
57. Moore, L. R. et al. Hemoglobin degradation in malaria-infected erythrocytes determined from live cell magnetophoresis. *FASEB J.* **20**, 747–749 (2006).
58. Peng, W. K. et al. Micromagnetic resonance relaxometry for rapid label-free malaria diagnosis. *Nat. Med.* **20**, 1069–1073 (2014).
59. Peng, W. K., Chen, L., Boehm, B. O., Han, J. & Loh, T. P. Molecular phenotyping of oxidative stress in diabetes mellitus with point-of-care nmr system. *NPJ Aging Mech. Dis.* **6**, 1–12 (2020).
60. Aime, S., Fasano, M., Paoletti, S., Arnelli, A. & Ascenzi, P. Nmr relaxometric investigation on human methemoglobin and fluoromethemoglobin. an improved quantitative in vitro assay of human methemoglobin. *Magn. Reson. Med.* **33**, 827–831 (1995).
61. Peng, W. K., Ng, T.-T. & Loh, T. P. Machine learning assistive rapid, label-free molecular phenotyping of blood with two-dimensional nmr correlational spectroscopy. *Commun. Biol.* **3**, 1–10 (2020).
62. Vu, C. et al. Reduced global cerebral oxygen metabolic rate in sickle cell disease and chronic anemias. *Am. J. Hematol.* **96**, 901–913 (2021).
63. Heidelberger, M., Mayer, M. M. & Demarest, C. R. Studies in human malaria: I. The preparation of vaccines and suspensions containing plasmodia. *J. Immunol.* **52**, 325–330 (1946).
64. Bohle, D. S., Debrunner, P., Jordan, P. A., Madsen, S. K. & Schulz, C. E. Aggregated heme detoxification byproducts in malarial trophozoites: β hematin and malaria pigment have a single s= 5/2 iron environment in the bulk phase as determined by epr and magnetic m¨ossbauer spectroscopy. *J. Am. Chem. Soc.* **120**, 8255–8256 (1998).
65. Sienkiewicz, A. et al. Multi-frequency high-field epr study of iron centers in malarial pigments. *J. Am. Chem. Soc.* **128**, 4534–4535 (2006).
66. Melville, D., Paul, F. & Roath, S. Direct magnetic separation of red cells from whole blood. *Nature* **255**, 706–706 (1975).
67. Fairlamb, A. H., Paul, F. & Warhurst, D. C. A simple magnetic method for the purification of malarial pigment. *Mol. Biochem. Parasitol.* **12**, 307–312 (1984).
68. Paul, F., Roath, S., Melville, D., Warhurst, D. & Osisanya, J. Separation of malaria-infected erythrocytes from whole blood: use of a selective high-gradient magnetic separation technique. *Lancet* **2**, 70–71 (1981).
69. Kim, C. C., Wilson, E. B. & DeRisi, J. L. Improved methods for magnetic purification of malaria parasites and haemozoin. *Malar. J.* **9**, 1–5 (2010).
70. Nam, J., Huang, H., Lim, H., Lim, C. & Shin, S. Magnetic separation of malaria-infected red blood cells in various developmental stages. *Anal. Chem.* **85**, 7316–7323 (2013).
71. Zborowski, M. et al. Red blood cell magnetophoresis. *Biophys. J.* **84**, 2638–2645 (2003).
72. Jaramillo, M. et al. Synthetic plasmodium-like hemozoin activates the immune response: a morphology-function study. *PloS ONE* **4**, 6957 (2009).
73. Ncokazi, K. K. & Egan, T. J. A colorimetric high-throughput β-hematin inhibition screening assay for use in the search for antimalarial compounds. *Anal. Biochem.* **338**, 306–319 (2005).
74. Butykai, A. et al. Malaria pigment crystals as magnetic micro-rotors: key for high-sensitivity diagnosis. *Sci. Rep.* **3**, 1–10 (2013).
75. Wang, X., Peng, W. & Lew, W. Flux-closure chirality control and domain wall trapping in asymmetric magnetic ring. *J. Appl. Phys.* **106**, 043905 (2009).
76. Gossuin, Y., Ndjolo, P. O., Vuong, Q. L. & Duez, P. Nmr relaxation properties of the synthetic malaria pigment β-hematin. *Sci. Rep.* **7**, 1–7 (2017).
77. Giacometti, M. et al. Electrical and magnetic properties of hemozoin nanocrystals. *Appl. Phys. Lett.* **113**, 203703 (2018).
78. Inyushin, M. et al. Superparamagnetic properties of hemozoin. *Sci. Rep.* **6**, 1–9 (2016).
79. Giacometti, M. et al. A lab-on-chip tool for rapid, quantitative, and stage-selective diagnosis of malaria. *Adv. Sci.* https://doi.org/10.1002/advs.202004101 (2021).
80. Lu, A.-H., Salabas, E. E. & Sch¨uth, F. Magnetic nanoparticles: synthesis, protection, functionalization, and application. *Angew. Chem. Int. Ed.* **46**, 1222–1244 (2007).
81. Kolhatkar, A. G., Jamison, A. C., Litvinov, D., Willson, R. C. & Lee, T. R. Tuning the magnetic properties of nanoparticles. *Int. J. Mol. Sci.* **14**, 15977–16009 (2013).
82. Schirhagl, R., Chang, K., Loretz, M. & Degen, C. L. Nitrogen-vacancy centers in diamond: nanoscale sensors for physics and biology. *Annu. Rev. Phys. Chem.* **65**, 83–105 (2014).
83. Doherty, M. W., Manson, N. B., Delaney, P. & Hollenberg, L. C. The negatively charged nitrogen-vacancy centre in diamond: the electronic solution. *N. J. Phys.* **13**, 025019 (2011).
84. Bhallamudi, V. P. & Hammel, P. C. Nanoscale MRI. *Nat. Nanotechnol.* **10**, 104–106 (2015).
85. Gould, M. et al. Room-temperature detection of a single 19 nm superparamagnetic nanoparticle with an imaging magnetometer. *Appl. Phys. Lett.* **105**, 072406 (2014).
86. Tetienne, J.-P. et al. Scanning nanospin ensemble microscope for nanoscale magnetic and thermal imaging. *Nano Lett.* **16**, 326–333 (2016).
87. Fescenko, I. et al. Diamond magnetic microscopy of malarial hemozoin nanocrystals. *Phys. Rev. Appl.* **11**, 034029 (2019).
88. Zimmerman, P. A., Thomson, J. M., Fujioka, H., Collins, W. E. & Zborowski, M. Diagnosis of malaria by magnetic deposition microscopy. *Am. J. Trop. Med. Hyg.* **74**, 568 (2006).
89. Kim, C., Hoffmann, G. & Searson, P. C. Integrated magnetic bead–quantum dot immunoassay for malaria detection. *ACS Sens.* **2**, 766–772 (2017).
90. Peng, W. K., Samoson, A. & Kitagawa, M. Simultaneous adiabatic spinlocking cross polarization in solid-state NMR of paramagnetic complexes. *Chem. Phys. Lett.* **460**, 531–535 (2008).
91. Peng, W. K. & Takeda, K. Efficient cross polarization with simultaneous adiabatic frequency sweep on the source and target channels. *J. Magn. Reson.* **188**, 267–274 (2007).
92. Karl, S., Guti´errez, L., House, M. J., Davis, T. M. & Pierre, T. G. S. Nuclear magnetic resonance: a tool for malaria diagnosis? *Am. J. Trop. Med. Hyg.* **85**, 815–817 (2011).
93. Peng, W. K., Chen, L. & Han, J. Development of miniaturized, portable magnetic resonance relaxometry system for point-of-care medical diagnosis. *Rev. Sci. Instrum.* **83**, 095115 (2012).
94. Han, J. & Peng, W. K. Reply to" considerations regarding the micromagnetic resonance relaxometry technique for rapid label-free malaria diagnosis". *Nat. Med.* **21**, 1387–1389 (2015).
95. Gupta, M. et al. A sensitive on-chip probe–based portable nuclear magnetic resonance for detecting low parasitaemia plasmodium falciparum in human blood. *Med. Devices Sens.* **3**, 10098 (2020).
96. Kong, T. F. et al. Enhancing malaria diagnosis through microfluidic cell enrichment and magnetic resonance relaxometry detection. *Sci. Rep.* **5**, 1–12 (2015).
97. Thamarath, S. S., Xiong, A., Lin, P.-H., Preiser, P. R. & Han, J. Enhancing the sensitivity of micro magnetic resonance relaxometry detection of low parasitemia *Plasmodium falciparum* in human blood. *Sci. Rep.* **9**, 1–9 (2019).
98. Di Gregorio, E. et al. Relaxometric studies of erythrocyte suspensions infected by *Plasmodium falciparum*: a tool for staging infection and testing anti-malarial drugs. *Magn. Reson. Med.* **84**, 3366–3378 (2020).
99. Veiga, M. I. & Peng, W. K. Rapid phenotyping towards personalized malaria medicine. *Malar. J.* **19**, 1–5 (2020).
100. Peng, W. K. Clustering nuclear magnetic resonance: machine learning assistive rapid two-dimensional relaxometry mapping. *Eng. Rep.* **3**, 12383 (2021).
101. Li, Y. et al. Magnetoresistance sensor with analog frontend for lab-on-chip malaria parasite detection. In: 2021 IEEE International Symposium on Circuits and Systems (ISCAS) (IEEE, 2021), pp. 1–5.
102. Milesi, F. et al. On-chip selective capture and detection of magnetic fingerprints of malaria. *Sensors* **20**, 4972 (2020).
103. Catarino, S. O. et al. Portable device for optical quantification of hemozoin in diluted blood samples. *IEEE Trans. Biomed. Eng.* **67**, 365–371 (2019).

104. Lawrence, C. & Olson, J. A. Birefringent hemozoin identifies malaria. *Am. J. Clin. Pathol.* **86**, 360–363 (1986).
105. B´elisle, J. M. et al. Sensitive detection of malaria infection by third harmonic generation imaging. *Biophys. J.* **94**, 26–28 (2008).
106. Burnett, J. L., Carns, J. L. & Richards-Kortum, R. In vivo microscopy of hemozoin: towards a needle free diagnostic for malaria. *Biomed. Opt. Express* **6**, 3462–3474 (2015).
107. Costa, M. S. et al. Multilayer thin-film optical filters for reflectance-based malaria diagnostics. *Micromachines* **12**, 890 (2021).
108. Campuzano-Zuluaga, G., H¨anscheid, T. & Grobusch, M. P. Automated haematology analysis to diagnose malaria. *Malar. J.* **9**, 1–15 (2010).
109. Shapiro, H. M., Ulrich, H. Cytometry in malaria: from research tool to practical diagnostic approach? (Wiley Online Library, 2010).
110. Cai, C. et al. In vivo photoacoustic flow cytometry for early malaria diagnosis. *Cytom. Part A* **89**, 531–542 (2016).
111. Wang, S., Yang, C., Preiser, P. & Zheng, Y. A photoacoustic-surfaceacoustic-wave sensor for ring-stage malaria parasite detection. *IEEE Trans. Circuits Syst. II* **67**, 881–885 (2020).
112. Wang, W. et al. Laser-induced surface acoustic wave sensing-based malaria parasite detection and analysis. *IEEE Trans. Instrum. Meas.* **71**, 1–9 (2021).
113. Kishor, R. et al. Microfluidic device based on opto-acoustics for particle concentration detection (2017).
114. Pourabed, A. et al. A star shaped acoustofluidic mixer enhances rapid malaria diagnostics via cell lysis and whole blood homogenisation in 2 seconds. *Lab a Chip* **22**, 1829–1840 (2022).
115. Lukianova-Hleb, E. Y. et al. Hemozoin-generated vapor nanobubbles for transdermal reagent-and needle-free detection of malaria. *Proc. Natl Acad. Sci. USA* **111**, 900–905 (2014).
116. Kazarine, A. et al. Malaria detection by third-harmonic generation image scanning cytometry. *Anal. Chem.* **91**, 2216–2223 (2019).
117. Tripathy, U. et al. Optimization of malaria detection based on third harmonic generation imaging of hemozoin. *Anal. Bioanal. Chem.* **405**, 5431–5440 (2013).
118. Wood, B. R. et al. Raman imaging of hemozoin within the food vacuole of *Plasmodium falciparum* trophozoites. *FEBS Lett.* **554**, 247–252 (2003).
119. Wood, B. R. et al. Resonance Raman spectroscopy reveals new insight into the electronic structure of β-hematin and malaria pigment. *J. Am. Chem. Soc.* **126**, 9233–9239 (2004).
120. Frosch, T., Koncarevic, S., Becker, K. & Popp, J. Morphology-sensitive Raman modes of the malaria pigment hemozoin. *Analyst* **134**, 1126–1132 (2009).
121. Wood, B. R. et al. Resonance raman microscopy in combination with partial dark-field microscopy lights up a new path in malaria diagnostics. *Analyst* **134**, 1119–1125 (2009).
122. Puskar, L. et al. Raman acoustic levitation spectroscopy of red blood cells and *Plasmodium falciparum* trophozoites. *Lab a Chip* **7**, 1125–1131 (2007).
123. Yuen, C. & Liu, Q. Magnetic field enriched surface enhanced resonance Raman spectroscopy for early malaria diagnosis. *J. Biomed. Opt.* **17**, 017005 (2012).
124. P´erez-Jim´enez, A. I., Lyu, D., Lu, Z., Liu, G. & Ren, B. Surface-enhanced raman spectroscopy: benefits, trade-offs and future developments. *Chem. Sci.* **11**, 4563–4577 (2020).
125. Garrett, N. L. et al. Bio-sensing with butterfly wings: naturally occurring nanostructures for users-based malaria parasite detection. *Phys. Chem. Chem. Phys.* **17**, 21164–21168 (2015).
126. Chen, K., Yuen, C., Aniweh, Y., Preiser, P. & Liu, Q. Towards ultrasensitive malaria diagnosis using surface enhanced Raman spectroscopy. *Sci. Rep.* **6**, 1–9 (2016).
127. Frosch, T. et al. In situ localization and structural analysis of the malaria pigment hemozoin. *J. Phys. Chem. B* **111**, 11047–11056 (2007).
128. Yuen, C. et al. Towards malaria field diagnosis based on surface-enhanced Raman scattering with on-chip sample preparation and near-analyte nanoparticle synthesis. *Sens. Actuators B* https://doi.org/10.1016/j.snb.2021.130162 (2021)
129. Wang, W. et al. Antibody-free rapid diagnosis of malaria in whole blood with surface enhanced Raman spectroscopy using nanostructured gold substrate. *Adv. Med. Sci.* **65**, 86–92 (2020).
130. Webster, G. T. et al. Discriminating the intraerythrocytic lifecycle stages of the malaria parasite using synchrotron ft-ir microspectroscopy and an artificial neural network. *Anal. Chem.* **81**, 2516–2524 (2009).
131. Wood, B. R. et al. Diagnosing malaria infected cells at the single cell level using focal plane array Fourier transform infrared imaging spectroscopy. *Analyst* **139**, 4769–4774 (2014).
132. Perez-Guaita, D. et al. High resolution ftir imaging provides automated discrimination and detection of single malaria parasite infected erythrocytes on glass. *Faraday Discuss.* **187**, 341–352 (2016).
133. Perez-Guaita, D. et al. Multispectral atomic force microscopy-infrared nanoimaging of malaria infected red blood cells. *Anal. Chem.* **90**, 3140–3148 (2018).
134. Khoshmanesh, A. et al. Detection and quantification of early-stage malaria parasites in laboratory infected erythrocytes by attenuated total reflectance infrared spectroscopy and multivariate analysis. *Anal. Chem.* **86**, 4379–4386 (2014).
135. Roy, S. et al. Simultaneous ATR-FTIR based determination of malaria parasitemia, glucose and urea in whole blood dried onto a glass slide. *Anal. Chem.* **89**, 5238–5245 (2017).
136. Martin, M. et al. The effect of common anticoagulants in detection and quantification of malaria parasitemia in human red blood cells by atr-ftir spectroscopy. *Analyst* **142**, 1192–1199 (2017).
137. Newman, D. M. et al. A magneto-optic route toward the in vivo diagnosis of malaria: preliminary results and preclinical trial data. *Biophys. J.* **95**, 994–1000 (2008).
138. Mens, P. F., Matelon, R. J., Nour, B. Y., Newman, D. M. & Schallig, H. D. Laboratory evaluation on the sensitivity and specificity of a novel and rapid detection method for malaria diagnosis based on magneto-optical technology (mot). *Malar. J.* **9**, 1–8 (2010).
139. Kumar, R. et al. First successful field evaluation of new, one minute haemozoin-based malaria diagnostic device. *EClinicalMedicine* **22**, 100347 (2020).
140. McBirney, S. E., Chen, D., Scholtz, A., Ameri, H. & Armani, A. M. Rapid diagnostic for point-of-care malaria screening. *ACS Sens.* **3**, 1264–1270 (2018).
141. Newman, D. M., Matelon, R. J., Wears, M. L. & Savage, L. B. The in vivo diagnosis of malaria: feasibility study into a magneto-optic fingertip probe. *IEEE J. Sel. Top. Quantum Electron.* **16**, 573–580 (2009).
142. Orb´an, A. et al. Evaluation of a novel magneto-optical method for the detection of malaria parasites. *PloS ONE* **9**, 96981 (2014).
143. Orb´an, A. et al. Efficient monitoring of the blood-stage infection in a malaria rodent model by the rotating-crystal magneto-optical method. *Sci. Rep.* **6**, 1–9 (2016).
144. Puk´ancsik, M. et al. Highly sensitive and rapid characterization of the development of synchronized blood stage malaria parasites via magnetooptical hemozoin quantification. *Biomolecules* **9**, 579 (2019).
145. Moln´ar, P. et al. Rapid and quantitative antimalarial drug efficacy testing via the magneto-optical detection of hemozoin. *Sci. Rep.* **10**, 1–11 (2020).
146. Roch, A., Prod´eo, J., Pierart, C., Muller, R. & Duez, P. The paramagnetic properties of malaria pigment, hemozoin, yield clues to a low-cost system for its trapping and determination. *Talanta* **197**, 553–557 (2019).
147. Traore, O. et al. Development and validation of an original magnetochromatography device for the whole blood determination of hemozoin, the paramagnetic malaria pigment. *Microchem. J.* **157**, 105043 (2020).
148. Zhang, T. et al. Toward quantitative bio-sensing with nitrogen–vacancy center in diamond. *ACS Sens.* **6**, 2077–2107 (2021).
149. Teeling-Smith, R. M. et al. Electron paramagnetic resonance of a single NV nanodiamond attached to an individual biomolecule. *Biophys. J.* **110**, 2044–2052 (2016).
150. Shi, F. et al. Singledna electron spin resonance spectroscopy in aqueous solutions. *Nat. Methods* **15**, 697–699 (2018).
151. Le Sage, D. et al. Optical magnetic imaging of living cells. *Nature* **496**, 486–489 (2013).
152. Glenn, D. R. et al. Single-cell magnetic imaging using a quantum diamond microscope. *Nat. Methods* **12**, 736–738 (2015).
153. Shi, F. et al. Singleprotein spin resonance spectroscopy under ambient conditions. *Science* **347**, 1135–1138 (2015).
154. Barry, J. F. et al. Optical magnetic detection of single-neuron action potentials using quantum defects in diamond. *Proc. Natl Acad. Sci. USA* **113**, 14133–14138 (2016).
155. Heraud, P. et al. Infrared spectroscopy coupled to cloud-based data management as a tool to diagnose malaria: a pilot study in a malaria-endemic country. *Malar. J.* **18**, 1–11 (2019).
156. Mwanga, E. P. et al. Detection of malaria parasites in dried human blood spots using mid-infrared spectroscopy and logistic regression analysis. *Malar. J.* **18**, 1–13 (2019).
157. de Melo, G. C. et al. Performance of a sensitive haemozoin-based malaria diagnostic test validated for vivax malaria diagnosis in Brazilian Amazon. *Malar. J.* **20**, 1–10 (2021).

158. Valdivia, H. O. et al. Field validation of a magneto-optical detection device (gazelle) for portable point-of-care plasmodium vivax diagnosis. *PloS ONE* **16**, 0253232 (2021).
159. Arndt, L. et al. Magneto-optical diagnosis of symptomatic malaria in Papua New Guinea. *Nat. Commun.* **12**, 1–10 (2021).
160. Wendt, C. et al. High-resolution electron microscopy analysis of malaria hemozoin crystals reveals new aspects of crystal growth and elemental composition. *Cryst. Growth Des.* **21**, 5521–5533 (2021).
161. Gruene, T., Holstein, J. J., Clever, G. H. & Keppler, B. Establishing electron diffraction in chemical crystallography. *Nat. Rev. Chem.* **5**, 660–668 (2021).
162. Guzm´an-Afonso, C. et al. Understanding hydrogen-bonding structures of molecular crystals via electron and nmr nanocrystallography. *Nat. Commun.* **10**, 1–10 (2019).
163. Mohorovic, L. et al. Methemoglobinemia—a biomarker and a link to ferric iron accumulation in Alzheimer's disease. *Adv. Biosci. Biotechnol.* **5**, 12–18 (2014).
164. Tejada, J., Zhang, X., Del Barco, E., Hernandez, J. & Chudnovsky, E. Macroscopic resonant tunneling of magnetization in ferritin. *Phys. Rev. Lett.* **79**, 1754 (1997).
165. Aggarwal, S., Peng, W. K. & Srivastava, S. Multi-omics advancements towards plasmodium vivax malaria diagnosis. *Diagnostics* **11**, 2222 (2021).
166. Dasgupta, R., Verma, R. S., Ahlawat, S., Uppal, A. & Gupta, P. K. Studies on erythrocytes in malaria infected blood sample with Raman optical tweezers. *J. Biomed. Opt.* **16**, 077009 (2011).
167. Sebba, D. et al. A point-of-care diagnostic for differentiating ebola from endemic febrile diseases. *Sci. Transl. Med.* **10**, 0944 (2018).
168. Jahn, I. et al. Surface-enhanced Raman spectroscopy and microfluidic platforms: challenges, solutions and potential applications. *Analyst* **142**, 1022–1047 (2017).
169. Veettil, T. C. P. et al. Disposable coverslip for rapid throughput screening of malaria using attenuated total reflection spectroscopy. *Appl. Spectrosc.* **76**, 451–461 (2022).
170. Adegoke, J. A., Kochan, K., Heraud, P. & Wood, B. R. A near-infrared "matchbox size" spectrometer to detect and quantify malaria parasitemia. *Anal. Chem.* **93**, 5451–5458 (2021).
171. Adegoke, J. A. et al. Ultraviolet/visible and near-infrared dual spectroscopic method for detection and quantification of low-level malaria parasitemia in whole blood. *Anal. Chem.* **93**, 13302–13310 (2021).
172. Adegoke, J. A., Raper, H., Gassner, C., Heraud, P. & Wood, B. R. Visible microspectrophotometry coupled with machine learning to discriminate the erythrocytic life cycle stages of p. falciparum malaria parasites in functional single cells. *Analyst* **147**, 2662–2670 (2022).
173. Rajaraman, S. et al. Pre-trained convolutional neural networks as feature extractors toward improved malaria parasite detection in thin blood smear images. *PeerJ* **6**, 4568 (2018).
174. Umer, M. et al. A novel stacked cnn for malarial parasite detection in thin blood smear images. *IEEE Access* **8**, 93782–93792 (2020).
175. Diker, A. An efficient model of residual based convolutional neural network with Bayesian optimization for the classification of malarial cell images. *Comput. Biol. Med.* **148**, 105635 (2022).
176. Sahlol, A. T., Kollmannsberger, P. & Ewees, A. A. Efficient classification of white blood cell leukemia with improved swarm optimization of deep features. *Sci. Rep.* **10**, 2536 (2020).
177. Cınar, A. & Tuncer, S. A. Classification of lymphocytes, monocytes, eosinophils, and neutrophils on white blood cells using hybrid alexnetgooglenet-svm. *SN Appl. Sci.* **3**, 1–11 (2021).
178. Zhang, K. et al. Machine learning-reinforced noninvasive biosensors for healthcare. *Adv. Healthc. Mater.* **10**, 2100734 (2021).
179. Cui, F., Yue, Y., Zhang, Y., Zhang, Z. & Zhou, H. S. Advancing biosensors with machine learning. *ACS Sens.* **5**, 3346–3364 (2020).
180. Ralbovsky, N. M. & Lednev, I. K. Towards development of a novel universal medical diagnostic method: Raman spectroscopy and machine learning. *Chem. Soc. Rev.* **49**, 7428–7453 (2020).
181. Tong, D. et al. Application of Raman spectroscopy in the detection of hepatitis b virus infection. *Photodiagn. Photodyn. Ther.* **28**, 248–252 (2019).
182. Naseer, K., Amin, A., Saleem, M. & Qazi, J. Raman spectroscopy based differentiation of typhoid and dengue fever in infected human sera. *Spectrochim. Acta Part A* **206**, 197–201 (2019).
183. Patel, S. K. et al. Rapid discrimination of malaria-and dengue-infected patients sera using Raman spectroscopy. *Anal. Chem.* **91**, 7054–7062 (2019).
184. Goulart, A. C. C. et al. Diagnosing covid-19 in human serum using Raman spectroscopy. *Lasers Med. Sci.* **37**, 2217–2226 (2022).
185. Nogueira, M. S. et al. Rapid diagnosis of COVID-19 using ft-ir atr spectroscopy and machine learning. *Sci. Rep.* **11**, 1–13 (2021).
186. Wood, B. R. et al. Infrared based saliva screening test for COVID-19. *Angew. Chem.* **133**, 17239–17244 (2021).
187. Chatzidrosos, G. et al. Miniature cavity-enhanced diamond magnetometer. *Phys. Rev. Appl.* **8**, 044019 (2017).
188. Webb, J. L. et al. Nanotesla sensitivity magnetic field sensing using a compact diamond nitrogen-vacancy magnetometer. *Appl. Phys. Lett.* **114**, 231103 (2019).
189. St¨urner, F. M. et al. Compact integrated magnetometer based on nitrogenvacancy centres in diamond. *Diam. Relat. Mater.* **93**, 59–65 (2019).
190. St¨urner, F. M. et al. Integrated and portable magnetometer based on nitrogen-vacancy ensembles in diamond. *Adv. Quantum Technol.* **4**, 2000111 (2021).
191. Burnett, J. L., Carns, J. L. & Richards-Kortum, R. Towards a needle-free diagnosis of malaria: in vivo identification and classification of red and white blood cells containing haemozoin. *Malar. J.* **16**, 1–12 (2017).
192. Aydin-Schmidt, B. et al. Usefulness of *Plasmodium falciparum*-specific rapid diagnostic tests for assessment of parasite clearance and detection of recurrent infections after artemisinin-based combination therapy. *Malar. J.* **12**, 1–11 (2013).
193. Serebrennikova, Y. M., Patel, J. & Garcia-Rubio, L. H. Interpretation of the ultraviolet-visible spectra of malaria parasite *Plasmodium falciparum*. *Appl. Opt.* **49**, 180–188 (2010).
194. Chaorattanakawee, S. et al. Direct comparison of the histidine-rich protein-2 enzyme-linked immunosorbent assay (hrp-2 elisa) and malaria SYBR green I fluorescence (MSF) drug sensitivity tests in *Plasmodium falciparum* reference clones and fresh ex vivo field isolates from Cambodia. *Malar. J.* **12**, 1–11 (2013).
195. Bacon, D. J. et al. Comparison of a SYBR green I-based assay with a histidine-rich protein ii enzyme-linked immunosorbent assay for in vitro antimalarial drug efficacy testing and application to clinical isolates. *Antimicrob. Agents Chemother.* **51**, 1172–1178 (2007).
196. Organization, W. H. et al. In vitro micro-test (mark iii) for the assessment of the response of plasmodium falciparum to chloroquine, mefloquine, quinine, amodiaquine, sulfadoxine. Technical report, World Health Organization (2001).
197. Webster, G. T., Tilley, L., Deed, S., McNaughton, D. & Wood, B. R. Resonance Raman spectroscopy can detect structural changes in haemozoin (malaria pigment) following incubation with chloroquine in infected erythrocytes. *FEBS Lett.* **582**, 1087–1092 (2008).
198. Wood, B. R. et al. Tip-enhanced Raman scattering (ters) from hemozoin crystals within a sectioned erythrocyte. *Nano Lett.* **11**, 1868–1873 (2011).
199. Kozicki, M. et al. An attenuated total reflection (atr) and Raman spectroscopic investigation into the effects of chloroquine on *Plasmodium falciparum*-infected red blood cells. *Analyst* **140**, 2236–2246 (2015).
200. Serebrennikova, Y. M. et al. Spectrophotometric detection of susceptibility to anti-malarial drugs. *Malar. J.* **12**, 1–9 (2013).
201. Rebelo, M. et al. A novel flow cytometric hemozoin detection assay for real-time sensitivity testing of *Plasmodium falciparum*. *PloS ONE* **8**, 61606 (2013).